UNLV Theses, Dissertations, Professional Papers, and Capstones

2009

Substituent effect on the electronic and assembling properties of asymmetric phenazine derivatives

Bin Cao
University of Nevada Las Vegas

SUBSTITUENT EFFECT ON THE ELECTRONIC AND

ASSEMBLING PROPERTIES OF ASYMMETRIC

PHENAZINE DERIVATIVES

by

Bin Cao

Bachelor of Engineering in Polymer Materials & Engineering
Zhengzhou University, China
2005

A thesis submitted in partial fulfillment
of the requirement for the

Master of Science Degree in Chemistry
Department of Chemistry
College of Sciences

Graduate College
University of Nevada, Las Vegas
August 2009

ABSTRACT

**Substituent Effect on the Electronic and Assembling Properties of
Asymmetric Phenazine Derivatives**

by

Bin Cao

Dr. Dong-Chan Lee, Exam Committee Chair
Assistant Professor of Chemistry
University of Nevada, Las Vegas

Currently, one-dimensional (1-D) nanostructures have drawn much interest because
of their potential applications for nanoscale optoelectronic devices. Self-assembly (SA)
based on π-conjugated systems through various intermolecular interactions has been
widely used to produce 1-D nanostructure. Morphology of the assembled structures can
be modified by incorporating substituents, which provide additional secondary
interactions. Meanwhile, those substituents also influence the electronic properties of the
molecules. Previous studies have made little effort to systematically study subsistent
effects on both electronic and SA properties.

The primary objective of this research is to generate controllable 1-D structures
through SA, and to provide a fundamental understanding of how different peripheral
substituents bonded to a π-core influence the electronic and assembling properties of the
molecules. A series of asymmetric phenazine derivatives containing different functional
groups were designed and synthesized in order to investigate the halogen effect, position
effect and the alkoxy chain length effect. The electronic properties were studied by UV-

vis spectroscopy, fluorescence spectroscopy, and cyclic voltammetry (CV). The experimental results of the systems' electronic properties are compared with the theoretical calculations. The SA properties were extensively investigated by polarized optical microscopy (POM), scanning electron microscopy (SEM), transmission electron microscopy (TEM), single crystal X-ray crystallography, and X-ray diffraction (XRD).

TABLE OF CONTENTS

LIST OF FIGURES

LIST OF ABBREVIATIONS

SA	Self-assembly
1-D	One-dimensional
OLED	Organic light emitting diode
HOMO	Highest occupied molecular orbital
LUMO	Lowest unoccupied molecular orbital
HB	Hydrogen bonding
XB	Halogen bonding
NMR	Nuclear magnetic resonance
MS	Mass spectrometry
CV	Cyclic voltammetry
PV	Photovoltaic
FET	Field effect transistor
SEM	Scanning electron microscopy
TEM	Transmission electron microscopy
BF	Bright field
STEM	Scanning transmission electron microscopy
HRTEM	High-resolution transmission electron microscopy
XRD	X-ray diffraction
TMS	Tetramethylsilane
DFT	Density functional theory
TD-DFT	Time-dependent density functional theory
PT	Phase transfer

ACKNOWLEDGEMENTS

First, I would like to thank my advisor, Dr. Dong-Chan Lee, for giving me this opportunity to work in his great lab, teaching me lots of useful knowledge and giving me good advices for my research.

Secondly, I would like to thank my labmates, Kyoungmi Jang, Kelly McGrath, Rycel Uy, and Vishal Patel for their help in the last two years. Especially I would like to thank Kyoungmi for her help with my samples' characterization.

I would like to express my gratitude to my thesis committee, Dr. Clemens Heske, Dr. Kathleen Robins, and Dr. Michael Pravica, for spending their time to review my thesis and for always being available when I had any questions.

I also appreciate Dr. Robins for performing theoretical calculations and taking time to explain the results to me. I would like to thank Dr. Paul Forster for providing us the single crystal X-ray crystallography and helping me to interpret the data. I would also like to thank Dr. David Hatchett for lending us a potentiostat for cyclic voltammetry measurements. I also express my gratitude to Dr. Longzhou Ma for obtaining TEM images of my samples. I would like to thank Dr. Yufeng Zhang and Lacie Brownell for helping me to check my thesis writing.

Lastly, I would like to thank my fiancée Linlin Li and my parents for their endless love and support through my time here at UNLV.

CHAPTER 1

SYNTHESES AND PHYSICAL PROPERTIES OF ASYMMETRIC

PHENAZINE DERIVATIVES

1.1. General Introduction

Most of electronic devices such as field effect transistors (FETs) and photovoltaic (PV) cells are based on inorganic semiconductors, and their organic counterparts have been relatively rare. However, organic semiconductors possess many advantages over their inorganic counterparts, such as optimizing their electronic structures by facile structure change, high flexibility, and low cost of device fabrication. One-dimensional (1-D) nanostructures such as nanofibers, nanobelts, nanotubes, etc., have gained increasing interest in both science and technology due to their potential applications in nanoscale optoelectronic devices.[1,2] The electronic properties and self-assembly (SA) abilities are the two important features if these materials are to be useful organic semiconductors. These two properties are the major focuses of this research.

SA based on π-conjugated systems through various intermolecular interactions has been widely used to induce 1-D structures.[3-5] SA is a spontaneous process by which molecules adopt well-defined superstructures through various noncovalent interactions such as hydrogen bonding (HB), halogen bonding (XB), π-π interactions, van der Waals forces, dipole-dipole interactions, etc. Previous studies of large macrocyclic aromatic molecules[3-7] such as hexabenzocoronene indicated that self-assembly through π-π

stacking could be an effective approach to 1-D nanostructures for planar, rigid organic molecules. However, in most cases different kinds of interactions such as HB, π-π interactions, and van der Waals forces exist simultaneously in a system and they cooperate with each other to assist SA. Consequently, rational molecular design is very important for successful growth of 1-D structures.

Due to the electron-withdrawing property of imine nitrogens, it has been demonstrated that the introduction of pyridine, pyrazine, or triazine containing heterocyclic moieties[8-11] could impart n-type character into the systems while their flat aromatic π core helps enhancing SA. The introduction of heteroaromatics cores should be a reasonable approach to achieve both electron-deficiency and self-assembly simultaneously. A number of imine containing heterocycles such as quinoline and quinoxaline have already been used as electron transporting material in organic light-emitting diodes (OLEDs).[8]

Another important issue is how to successfully control both electronic properties and morphologies with different substituents. It has been reported that incorporating electron-withdrawing substituents such as cyano (CN) and fluorine (F) into p-type semiconductors can create new n-type structural analogues.[12-17] Also, manipulating the side groups[18-21] connected to the π-core can provide additional secondary interactions,[22, 23] which is a good way to accomplish the morphology control.

Published works from our lab shows that two kinds of heteroaromatic asymmetric bisphenazine derivatives demonstrate excellent self-assembly properties.[24-27] Therefore, to provide further understanding on the SA of heteroaromatic compounds, this thesis will focus on substituent effect on the electronic and assembling properties of asymmetric

phenazines derivatives. A total of eight molecules will be presented and their electronic characters and assembling morphologies will be discussed. These molecules are designed based on a heteroaromatic phenazine π-core that can easily be substituted peripherally to further tune its assembly and electronic properties.

1.2. Molecular Design

In this research, phenazine was chosen as a platform for its assembling ability and electron-deficiency. It has been reported that the substituted dialkoxy phenazine exhibits gelling properties and shows potential as an acid-sensor.[28] Previous studies on other π system have corroborated the fact that slight modification of an aromatic ring can have a remarkable influence on both physical properties and molecular arrangement, and may further change the morphology of the assembled structures.[26,27,29,30] However, to the best of our knowledge, the effect of substituents on phenazine has not been extensively studied. Due to its SA ability and better electron-dificiency nature compared to anthracene, further investigation of the phenazine moiety, a potentially promising n-type semiconductor,[31] requires a facile synthetic route and a sensible molecular design.

Eight asymmetric phenazine derivatives were designed and synthesized to study both electronic character and 1-D SA (Figure 1.1). Three major structural features are of importance in this design. First, phenazine is a planar heteroaromatic molecule that may assist self-assembly through π-π interactions. Compared to previous reported π system,[3,4,24-27] phenazine has a smaller π core which may provide less efficient π orbital overlap. However, π-π stacking is not the only driving force to induce SA, and the

3

additional interactions including HB, XB, and van der Waals interactions will support SA. In addition, the presence of two imine nitrogens makes the system electron-deficient.
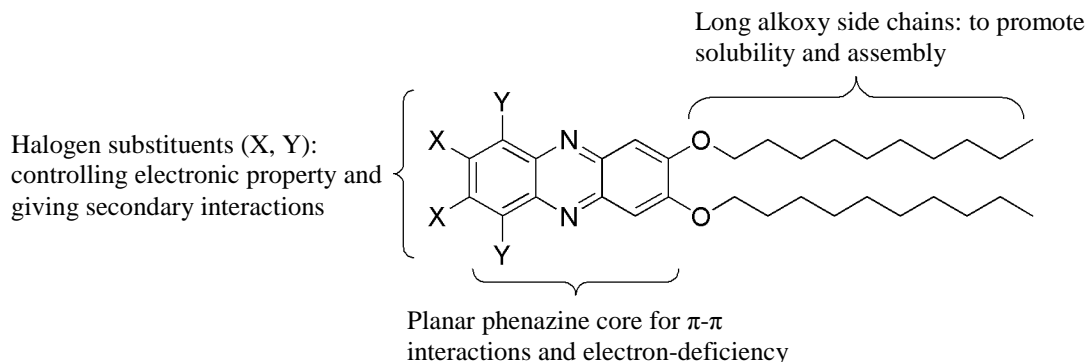
Figure 1.1. Design principle of asymmetrically substituted phenazines

The π-core is substituted asymmetrically by two different types of substituents. Long alkoxy chains with variable length are attached to one side of the π-core to promote solubility and assembly through cooperative van der Waals interactions. The halogen substituents added to the other side vary in size, position, and electron-withdrawing ability. These substituents will further tune the electronic properties such as electron-deficiency and HOMO-LUMO energy gap while modulating the morphology of assembly. Overall, this design strategy will allow for the SA through cooperation of different intermolecular interactions while tuning the electronic properties of the molecule by changing the peripheral substituents.

The first chapter will focus on the synthesis and physical properties of the molecules including optical and electrochemical characters. The subsequent chapter will focus on the molecular packing and assembly morphology of the final compounds through a study of cast film and solution based 1-D assembly using a phase transfer (PT) method.

1.3. Instrumentation

Nuclear magnetic resonance (NMR) spectra were obtained at 25 °C on a Varian Gemini 400 MHz spectrometer. Deuterated chloroform ($CDCl_3$) with tetramethylsilane (TMS) as an internal standard was used as the solvent for all samples. Mass spectrometry (MS) data was collected at the University of North Carolina Chapel Hill and University of Illinois at Chicago. UV-vis absorption spectra of the final products were collected on a Shimadzu UV-2450 UV-vis spectrophotometer from solutions in CH_2Cl_2. Fluorescence emission spectra were obtained on a Horiba Flourescencemeter using a xenon lamp for excitation. Data was obtained from much diluted solutions in CH_2Cl_2 with excitation at different wavelengths. Cyclic voltammetry (CV) was performed on a CH Instrument 660C potentiostat using a 3-electrode cell with a platinum disc working electrode (2 mm diameter), a nonaqueous Ag/Ag^+ reference electrode (Ag^+ as 10 mM $AgNO_3$ solution in anhydrous acetonitrile), and a platinum plate as the counter electrode. CV measurements for all compounds were obtained from a methylene chloride solution of the compound in 0.1 M tetrabutylammonium hexafluorophosphate ($TBAPF_6$) as the supporting electrolyte. The electrolyte solution containing the sample was purged with Ar for 15 - 20 minutes before each experiment and a blanket of Ar was used during the measurements. The scan rate was adjusted to 100 mV for all experiments. All potentials were calibrated to the ferrocene/ferrocenium (Fc/Fc^+) redox couple.

1.4. Synthesis Procedures

All chemicals and solvents were purchased from chemical sources and used as received. The target molecules (**1** - **8**) were prepared by the procedure shown in section 1.5.1 (Scheme 1). All the compounds were confirmed by ^{1}H-NMR, ^{13}C-NMR and mass spectrometry.

Compound 1

1,2-Diaminobenzene (100 mg, 0.93 mmol) was dissolved in 20 mL absolute ethanol. 2,5-Dihydroxyl-1,4-benzoquinone (130 mg, 0.93 mmol) was added at once and the mixture was refluxed for 24 hours under a positive N_2 flow. The reaction mixture was cooled slightly. Without purification of the intermediate, after evaporating the solvent, the crude solid was dissolved in 20 mL dimethylformamide (DMF), followed by addition of K_2CO_3 (447 mg, 3.23 mmol). Then bromodecane (616 mg, 0.58 mL) was added and the mixture was maintained at 60 ˚C for 24 hrs with continuous stirring. The mixture was cooled down to room temperature and poured into 200 mL of H_2O, filtered and washed thoroughly with H_2O. It was then dried over anhydrous sodium sulfate. The product was purified by silica gel column chromatography (CH_2Cl_2/Hexane 1/2 v/v). The pure product was obtained as a yellow solid. (Two-step yield: 58%).

^{1}H NMR (CDCl$_3$) δ 8.14 (m, 2H), 7.73 (m, 2H), 7.35 (s, 2H), 4.23 (t, 4H, J = 6.6 Hz), 1.96 (m, 4H), 1.54 (m, 4H), 1.5-1.2 (m, 24H), 0.89 (t, 6H, J = 6.8 Hz).

^{13}C NMR (CDCl$_3$) δ 154.48, 142.01, 141.84, 128.81, 105.54, 69.30, 31.92, 29.62, 29.58, 29.37, 29.36, 28.73, 26.05, 22.70, 14.12. (1 aromatic peak not seen due to overlapping signals)

[M+H]$^+$: Calcd 493.37; Found 493.3.

Compound 2

1,2-Diamino-4,5-diflurobenzene (50 mg, 0.35 mmol) was dissolved in 7 mL absolute ethanol. 2,5-Dihydroxyl-1,4-benzoquinone (49 mg, 0.35 mmol) was added at once and the mixture was refluxed for 24 hours under a positive N_2 flow. The reaction mixture was cooled slightly. After evaporating the solvent, without purification of the intermediate, the crude solid was dissolved in 8 mL DMF, followed by addition of K_2CO_3 (168 mg, 1.23 mmol). Then bromodecane (231 mg, 0.22 mL) was added and the mixture was maintained at 60 °C for 24 hrs with continuous stirring. The mixture was cooled down to room temperature and poured into 80 mL of H_2O, filtered and washed thoroughly with H_2O. It was then dried over anhydrous sodium sulfate. The product was purified by silica gel column chromatography (CH_2Cl_2/Hexane 1/6 v/v). The pure product was obtained as a white solid. (Two-step yield: 68%).

^{1}H NMR (CDCl$_3$) δ 7.84 (dd, 2H, J = 9.6 Hz), 7.30 (s, 2H), 4.22 (t, 4H, J = 6.6 Hz), 1.96 (m, 4H), 1.54 (m, 4H), 1.5-1.2 (m, 24H), 0.89 (t, 6H, J = 7 Hz).

^{13}C NMR (CDCl$_3$) δ 154.75, dd (153.56, 153.37, 151.00, 150.80), 141.88, t (139.02, 138.96, 138.91), q (113.65, 113.58, 113.52, 113.45), 105.28, 69.39, 31.93, 29.62, 29.58, 29.36, 28.72, 26.04, 22.70, 14.12. (1 aliphatic peak not seen due to overlapping signals)

[M+H]$^+$: Calcd 529.35; Found 529.3.

Compound 3

1,2-Diamino-4,5-dichlorobenzene (177 mg, 1 mmol) was dissolved in 25 mL absolute ethanol. 2,5-Dihydroxyl-1,4-benzoquinone (140 mg, 1 mmol) was added at once and the mixture was refluxed for 24 hours under a positive N_2 flow. The reaction mixture was cooled slightly. After evaporating the solvent, without purification of the intermediate,

the crude solid was dissolved in 20 mL DMF, followed by addition of K_2CO_3 (493 mg, 3.5 mmol). Then bromodecane (676 mg, 0.64 mL) was added and the mixture was maintained at 60 ˚C for 24 hrs with continuous stirring. The mixture was cooled down to room temperature and poured into 200 mL of H_2O, filtered and washed thoroughly with H_2O. It was then dried over anhydrous sodium sulfate. The product was purified by silica gel column chromatography (CH_2Cl_2/Hexane 1/3 v/v). The pure product was obtained as a yellow solid. (Two-step yield: 44%).

^{1}H NMR (CDCl$_3$) δ 7.94 (s, 2H), 7.00 (s, 2H), 4.10 (t, 4H, $J = 6.6$ Hz), 1.94 (m, 4H), 1.54 (m, 4H), 1.5-1.2 (m, 24H), 0.89 (t, 6H, $J = 6.8$ Hz).

^{13}C NMR (CDCl$_3$) δ 154.98, 142.16, 139.81, 132.75, 128.90, 105.10, 69.31, 31.96, 29.68, 29.64, 29.45, 29.41, 28.80, 26.08, 22.73, 14.14.

[M+H]$^{+}$: Calcd 561.29; Found 561.5.

Compound 4

1,2-Diamino-4,5-dibromobenzene (500 mg, 1.88 mmol) was dissolved in 40 mL absolute ethanol. 2,5-Dihydroxyl-1,4-benzoquinone (260 mg, 1.88 mmol) was added at once and the mixture was refluxed for 24 hours under a positive N_2 flow. The reaction mixture was cooled slightly. After evaporating the solvent, without purification of the intermediate, the crude solid was dissolved in 40 mL DMF, followed by addition of K_2CO_3 (910 mg, 6.5 mmol). Then bromodecane (820 mg, 0.77 mL) was added and the mixture was maintained at 60 ˚C for 24 hrs with continuous stirring. The mixture was cooled down to room temperature and poured into H_2O, filtered and washed thoroughly with H_2O. It was then dried over anhydrous sodium sulfate. The product was purified by silica gel column

chromatography (CH$_2$Cl$_2$/Hexane 1/1 v/v). The pure product was obtained as a yellow solid. (Two-step yield: 57%).

^{1}H NMR (CDCl$_3$) δ 8.45 (s, 2H), 7.27 (s, 2H), 4.22 (t, 4H, J = 6.6 Hz), 1.95 (m, 4H), 1.54 (m, 4H), 1.5-1.2 (m, 24H), 0.88 (t, 6H, J = 6.8 Hz).

^{13}C NMR (CDCl$_3$) δ 155.28, 142.58, 140.72, 132.59, 124.97, 105.32, 69.44, 31.92, 29.63, 29.58, 29.36, 28.71, 26.03, 22.70, 14.12. (1 aliphatic peak not seen due to overlapping signals)

[M]$^+$: Calcd 648.19; Found 648.3.

Compound 5

1,2-Diamino-4,5-diiodobenzene (366 mg, 1.02 mmol) was dissolved in 25 mL absolute ethanol. 2,5-Dihydroxyl-1,4-benzoquinone (143 mg, 1.02 mmol) was added at once and the mixture was refluxed for 24 hours under a positive N$_2$ flow. The reaction mixture was cooled slightly. After evaporating the solvent, without purification of the intermediate, the crude solid was dissolved in 20 mL DMF, followed by addition of K$_2$CO$_3$ (493 mg, 3.5 mmol). Then bromodecane (676 mg, 0.64 mL) was added and the mixture was maintained at 60 °C for 24 hrs with continuous stirring. The mixture was cooled down to room temperature and poured into 200 mL of H$_2$O, filtered and washed thoroughly with H$_2$O. It was then dried over anhydrous sodium sulfate. The product was purified by silica gel column chromatography (CH$_2$Cl$_2$/Hexane 1/2 v/v). The pure product was obtained as a yellow solid. (Two-step yield: 54%).

^{1}H NMR (CDCl$_3$) δ 8.64 (s, 2H), 7.18 (s, 2H), 4.20 (t, 4H, J = 6.6 Hz), 1.95 (m, 4H), 1.54 (m, 4H), 1.5-1.2 (m, 24H), 0.88 (t, 6H, J = 6.8 Hz).

^{13}C NMR (CDCl$_3$) δ 155.28, 142.46, 141.17, 138.84, 107.33, 105.34, 69.41, 31.92, 29.63, 29.58, 29.37, 29.36, 28.72, 26.04, 22.70, 14.12.

[M+H]$^+$: Calcd 745.16; Found 745.1.

Compound 6:

1,2-Diamino-3,6-dibromobenzene (676 mg, 2.54 mmol) was dissolved in 55 mL absolute ethanol. 2,5-Dihydroxyl-1,4-benzoquinone (356 mg, 2.54 mmol) was added at once and the mixture was refluxed for 24 hours under a positive N$_2$ flow. The reaction mixture was cooled slightly. After evaporating the solvent, without purification of the intermediate, the crude solid was dissolved in 50 mL DMF, followed by addition of K$_2$CO$_3$ (1.23 g, 8.89 mmol). Then bromodecane (1.13 g, 1.06 mL) was added and the mixture was maintained at 60 ˚C for 24 hrs with continuous stirring. The mixture was cooled down to room temperature and poured into 500 mL of H$_2$O, filtered and washed thoroughly with H$_2$O. It was then dried over anhydrous sodium sulfate. The product was purified by silica gel column chromatography (CH$_2$Cl$_2$/Hexane 1/2 v/v). The pure product was obtained as a yellow solid. (Two-step yield: 56%).

^{1}H NMR (CDCl$_3$) δ 7.93 (s, 2H), 7.48 (s, 2H), 4.25 (t, 4H, J = 6.6 Hz), 1.97 (m, 4H), 1.54 (m, 4H), 1.41-1.28 (m, 24H), 0.89 (t, 6H, J = 6.8 Hz).

^{13}C NMR (CDCl$_3$) δ 155.64, 142.78, 139.51, 131.57, 123.20, 105.45, 69.63, 31.92, 29.60, 29.57, 29.36, 29.33, 28.73, 26.00, 22.70, 14.13.

[M+H]$^+$: Calcd 651.19; Found 651.1.

Compound 7:

1,2-Diamino-4,5-diiodobenzene (400 mg, 1.11 mmol) was dissolved in 25 mL absolute ethanol. 2,5-Dihydroxyl-1,4-benzoquinone (156 mg, 1.11 mmol) was added at once and

the mixture was refluxed for 24 hours under a positive N_2 flow. The reaction mixture was cooled slightly. After evaporating the solvent, without purification of the intermediate, the crude solid was dissolved in 22 mL DMF, followed by addition of K_2CO_3 (537 mg, 3.89 mmol). Then bromohendecane (783 mg, 0.75 mL) was added and the mixture was maintained at 60 °C for 24 hrs with continuous stirring. The mixture was cooled down to room temperature and poured into 250 mL of H_2O, filtered and washed thoroughly with H_2O. It was then dried over anhydrous sodium sulfate. The product was purified by silica gel column chromatography (CH_2Cl_2/Hexane 1/2 v/v). The pure product was obtained as a yellow solid. (Two-step yield: 71%).

^{1}H NMR (CDCl$_3$) δ 8.70 (s, 2H), 7.24 (s, 2H), 4.21 (t, 4H, $J = 6.6$ Hz), 1.95 (m, 4H), 1.54 (m, 4H), 1.5-1.2 (m, 28H), 0.88 (t, 6H, $J = 6.4$ Hz).

^{13}C NMR (CDCl$_3$) δ 155.58, 142.82, 141.55, 139.14, 107.59, 105.60, 69.67, 32.16, 29.87, 29.84, 29.60, 29.57, 28.91, 26.23, 22.92, 14.34. (1 aliphatic peak not seen due to overlapping signals)

[M]$^+$: Calcd 772.20; Found 772.3.

Compound 8:

1,2-Diamino-4,5-diiodobenzene (400 mg, 1.11 mmol) was dissolved in 25 mL absolute ethanol. 2,5-Dihydroxyl-1,4-benzoquinone (156 mg, 1.11 mmol) was added at once and the mixture was refluxed for 24 hours under a positive N_2 flow. The reaction mixture was cooled slightly. After evaporating the solvent, without purification of the intermediate, the crude solid was dissolved in 22 mL DMF, followed by addition of K_2CO_3 (537 mg, 3.89 mmol). Then bromohendecane (1.02 g, 1.02 mL) was added and the mixture was maintained at 60 °C for 24 hrs with continuous stirring. The mixture was cooled down to

room temperature and poured into 250 mL of H_2O, filtered and washed thoroughly with H_2O. It was then dried over anhydrous sodium sulfate. The product was purified by silica gel column chromatography (CH_2Cl_2/Hexane 1/2 v/v). The pure product was obtained as a yellow solid. (Two-step yield: 60%).

^{1}H NMR (CDCl$_3$) δ 8.72 (s, 2H), 7.25 (s, 2H), 4.22 (t, 4H, J = 6.6 Hz), 1.95 (m, 4H), 1.54 (m, 4H), 1.5-1.2 (m, 48H), 0.88 (t, 6H, J = 6.8 Hz).

^{13}C NMR (CDCl$_3$) δ 155.38, 142.63, 141.37, 138.95, 107.39, 105.40, 69.46, 31.94, 29.73, 29.71, 29.68, 29.62, 29.38, 29.35, 28.69, 26.02, 22.70, 14.13. (4 aliphatic peaks not seen due to overlapping signals)

[M]$^+$: Calcd 912.35; Found 912.3.

1.5. Results and Discussion

1.5.1. Synthesis
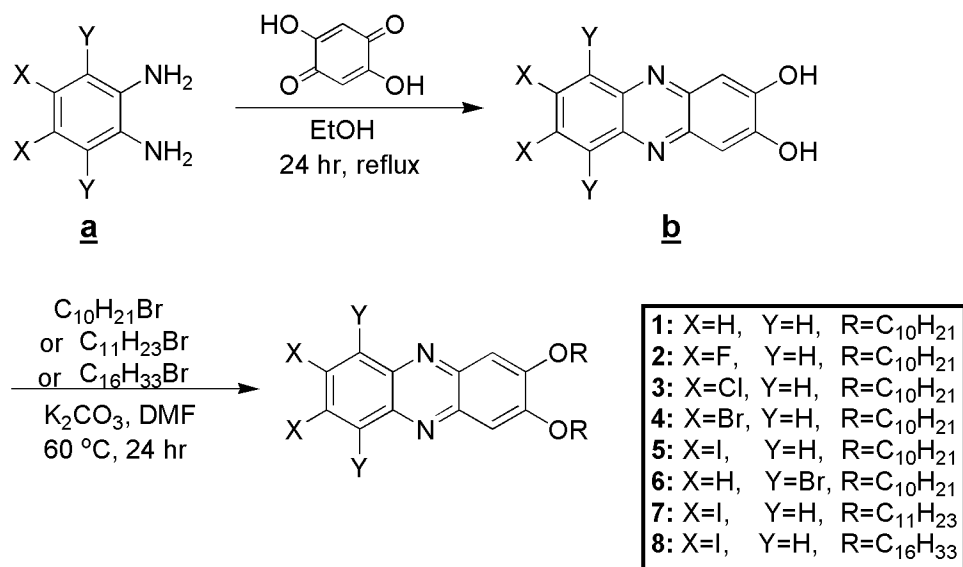
Scheme 1. Sequential synthetic route to compounds **1 – 8**.

The route to synthesis of final compounds **1–8** is described in Scheme 1, following the literature report.[28] As mentioned in the previous section, for the first step of synthesizing title compounds (**1–8**), the dihydroxyphenazine intermediate was yielded after a cyclization. Due to the presence of hydroxyl groups in compound **b**, column chromatography could not be used for purification owing to the strong OH interactions with the silica gel. The crude product was subjected to a Williamson Ether Synthesis to yield the final product. Except for compound **3**, good yields (two steps overall yield) above 50% were obtained for all other compounds.
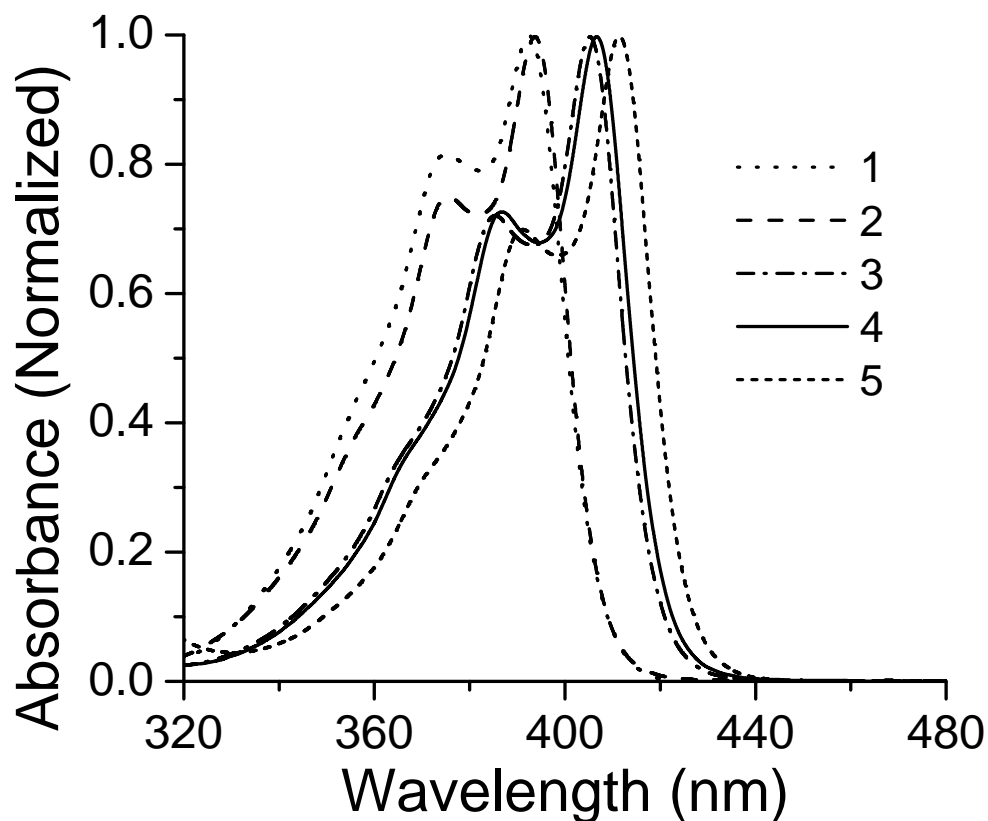
Figure 1.2. Normalized UV-vis spectra for final compounds **1**–**5**.

The UV-vis spectra for compounds **1-5** are shown in Figure 1.2. The spectra have been normalized at the absorption maxima of each compound for comparison. All of the final compounds showed absorption maxima around 380 to 410 nm arising from the aromatic phenazine core. The absorption edge is gradually shifted to longer wavelengths as the substituent is changed from H (**1**) to F (**2**) to Cl (**3**) to Br (**4**) to I (**5**). As a result, the HOMO-LUMO energy gap calculated from the tangent of the absorption edge[32] decreases in the same order (Table 1). The UV-vis absorption results show that the

electronic properties of this series of phenazine derivatives can be modulated with different halogen substituents.
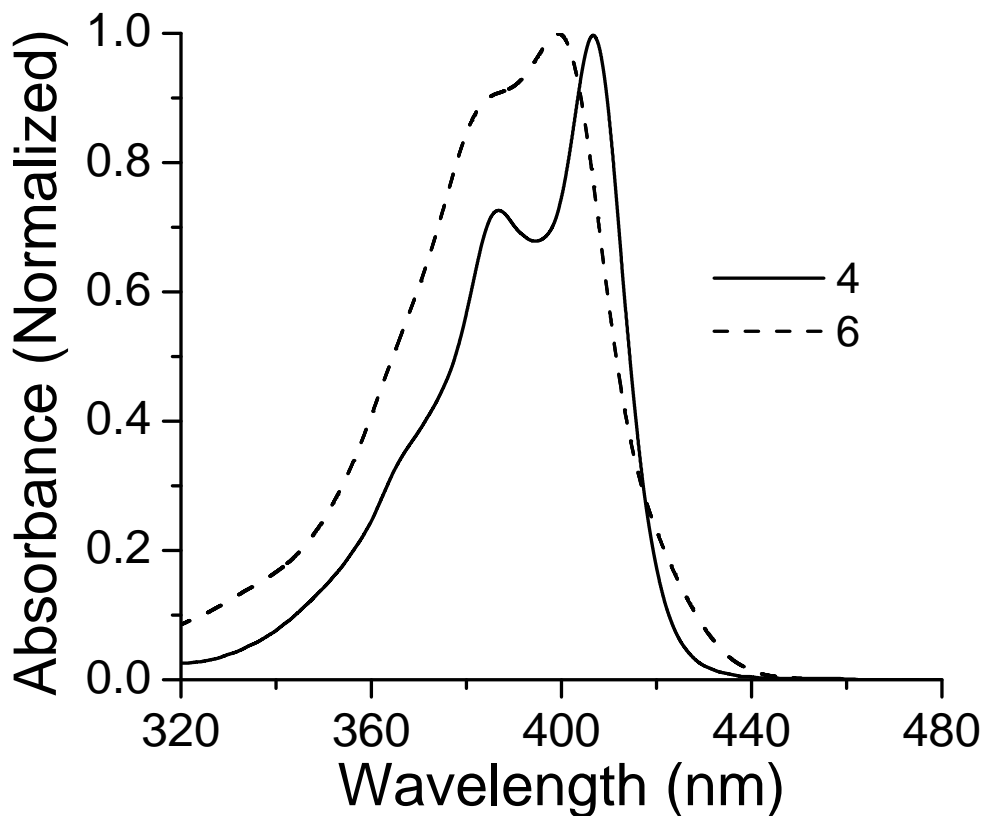
Figure 1.3. Normalized UV-vis spectra for final compounds **4** and **6**.

The UV-vis spectra comparison of compounds **4** and **6** are shown in Figure 1.3. The absorption edge is shifted to longer wavelengths as the bromine substituents switched from 2,3- to 1,4-position. As a result, the HOMO-LUMO energy gaps were decreased in the same order.

The absorption spectra of compounds **5**, **7** and **8** were nearly identical. This was expected because changing the alkoxy chain length of the side group does not affect the molecules chromophore.
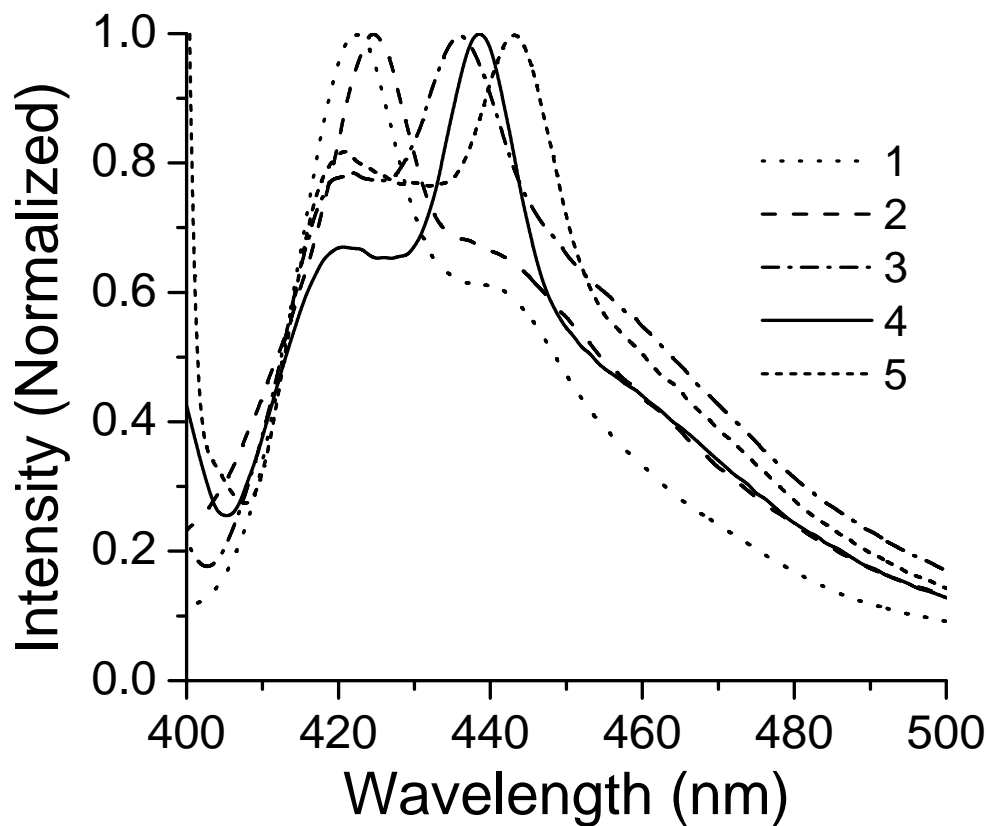
Figure 1.4. Normalized fluorescence spectra for final compounds **1**–**5**. Excitation λ: 375 nm (**1**), 376 nm (**2**), 385 nm (**3**), 387 nm (**4**), and 391 nm (**5**).

The fluorescence emission spectra for compounds **1-5** are shown in Figure 1.4. The fluorescence spectra have been normalized at the emission maxima for comparison. The reduction of the optical energy gap seen in the UV-vis spectra shows the same trend in fluorescence. As the HOMO-LUMO gap becomes smaller, the emission maxima in the fluorescence spectra were shifted to longer wavelengths which can be clearly seen in the spectra.
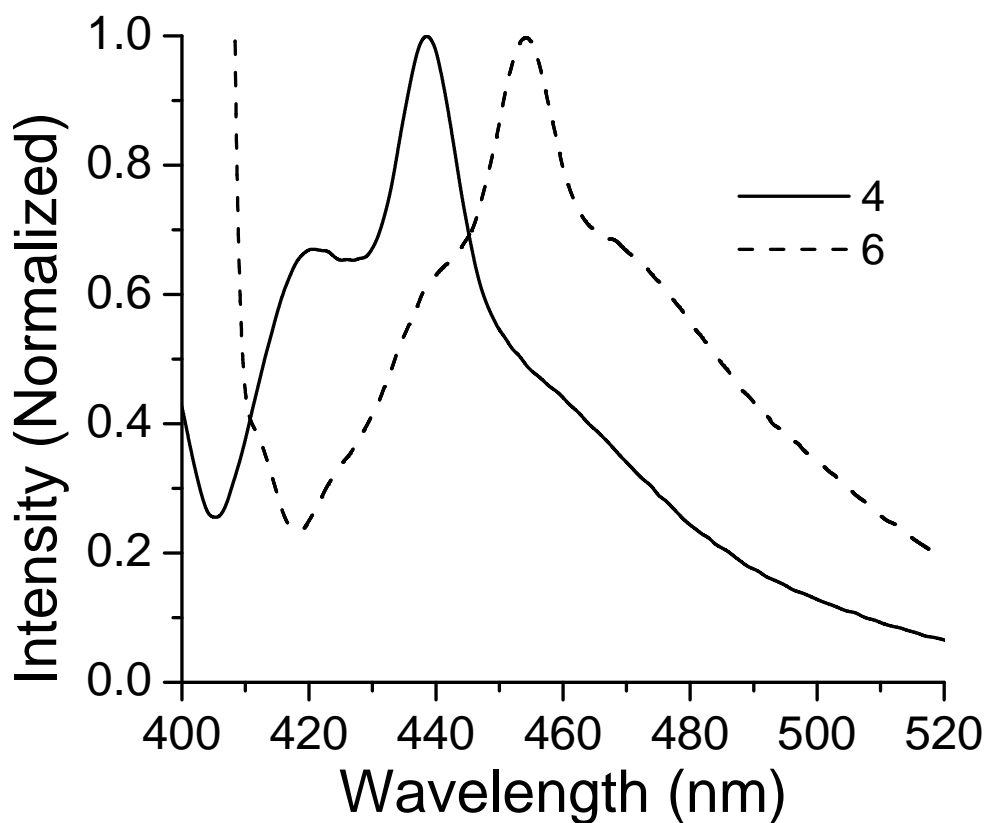
Figure 1.5. Normalized fluorescence spectra for final compounds **4** and **6**. Excitation λ: 387 nm (**4**), and 399 nm (**6**).

The fluorescence emission spectra comparison of compounds **4** and **6** are shown in Figure 1.5. The λ$_{max}$ was shifted from 438 nm (**4**) to 454 nm (**6**), so the energy gap of compound **6** (1,4-disubstituted) was smaller than compound **4** (2,3-disubstituted).

There were still no differences in the emission spectra of compounds **5**, **7** and **8**. This was due to the same effect observed in UV-vis; changing the length of the alkoxy side groups has no effect on its optical properties.

1.5.4. Cyclic voltammetry
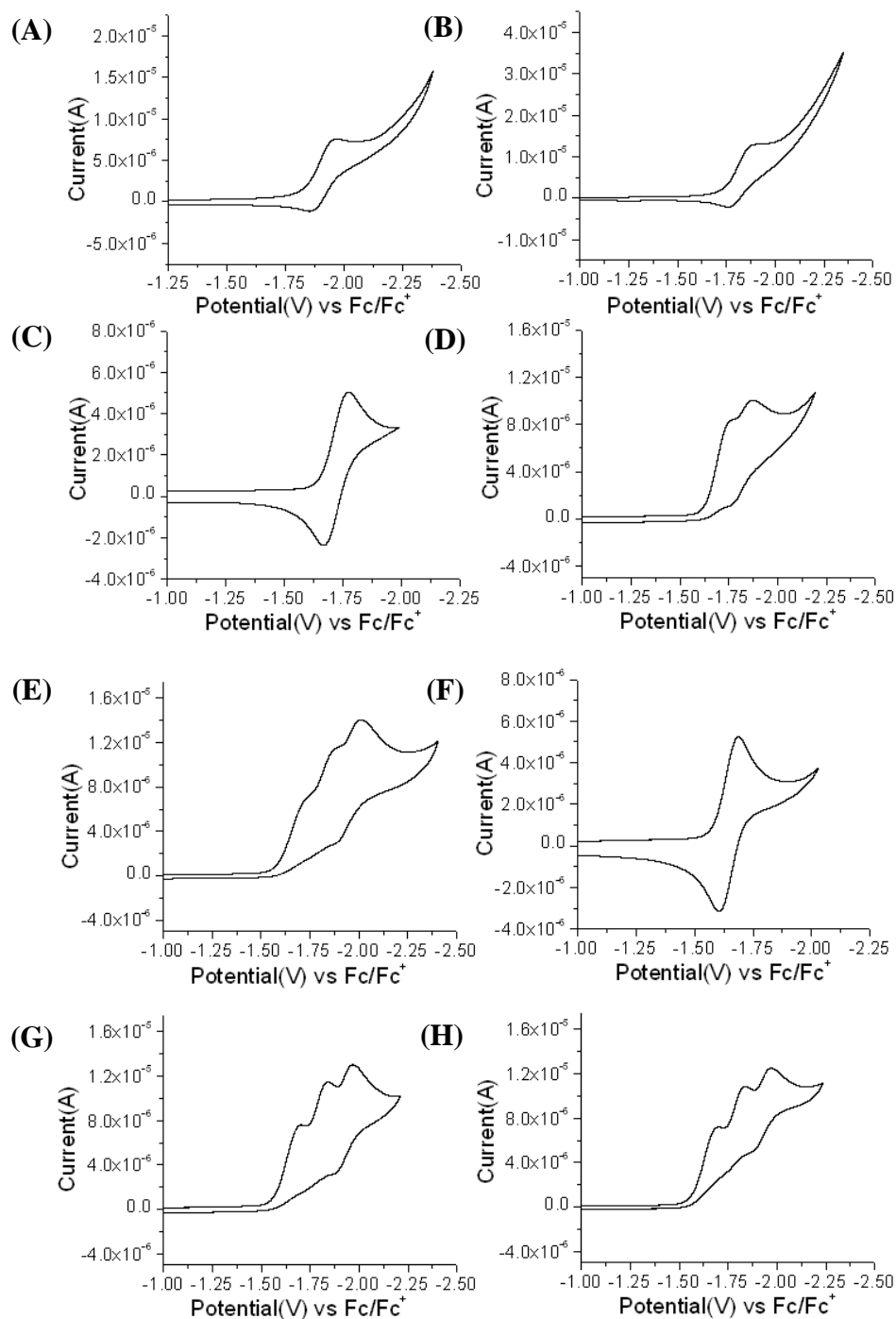
Figure 1.6. Cyclic Voltammograms for the reduction of **1** (A), **2** (B), **3** (C), **4** (D), **5** (E), **6** (F), **7** (G) and **8** (H). Scan rate: 100mV/s

The electrochemical properties of all eight compounds were studied with cyclic voltammetry (Figure 1.6). Our primary concern was the first reduction potential which can be directly related to the LUMO level of the molecules. Thus the onset of the first reduction wave was measured to calculate the LUMO energy (Table 1.1).

In this series of compounds, the LUMO level was continuously decreased as the electron-withdrawing ability of the substituent increased: **1** < **2** < **3** < **4** < **5** = **7** = **8** and as the position of bromine substituents changed from 2,3- to 1,4-position**.** These results demonstrate that increasing the electron-affinity of a whole system can be accomplished by introducing proper peripheral substituents to the phenazine moiety.

The onset of the first oxidation wave can similarly be used to calculate the HOMO level of the molecules; however, we were not able to obtain the accurate oxidation potentials of those compounds because of overlap with the solvent background. Thus, HOMO levels could not be directly estimated from CV. Instead, HOMO energies associated with the molecules with different functional groups were estimated from the LUMO energies in combination with the HOMO/LUMO energy gaps derived from the UV-vis spectroscopy (Table 1.1).

Theoretical calculations were performed to compare with the experimental LUMO levels obtained from CV and energy band gap results obtained from UV-vis spectroscopy. Optimum geometries were calculated with the density functional theory (DFT) at the B3LYP/6-31G* level and HOMO and LUMO energies were predicted by single point calculation (B3LYP/6-31+G*//B3LYP/TD-DFT 6-31G*). Time-dependent density functional theory (TD-DFT) was also employed for the energy gap computation

(B3LYP/6-31+G*). These values are summarized and compared with experimental results in Table 1.1.

Table 1. Electronic properties of compounds **1 – 8** from experimental data and theoretical calculations.

| | E_{red}^{peak} | E_{red}^{onset} | E_{LUMO} [a] | E_{HOMO} [b] | E_{gap} [c] | E_{LUMO} [d] | E_{HOMO} [d] | E_{gap} [d] |
	[V]	[V]	[eV]	[eV]	[eV]	[eV]	[eV]	[eV]
1	-1.97	-1.81	-2.99	-5.91	2.92	-2.27	-5.52	3.25
2	n/a[e]	-1.73	-3.07	-5.99	2.92	-2.52	-5.77	3.25
3	-1.77	-1.62	-3.18	-6.09	2.91	-2.62	-5.75	3.13
4	n/a[e]	-1.58	-3.22	-6.12	2.90	-2.64	-5.77	3.13
5	n/a[e]	-1.52	-3.28	-6.06	2.78	n/a[f]	n/a[f]	n/a[f]
6	-1.69	-1.54	-3.26	-6.09	2.83	-2.66	-5.65	2.99
7	n/a[e]	-1.52	-3.28	-6.06	2.78	n/a[f]	n/a[f]	n/a[f]
8	n/a[e]	-1.52	-3.28	-6.06	2.78	n/a[f]	n/a[f]	n/a[f]

[a] $E_{LUMO} = -(E_{red}^{onset} + 4.8 \text{ eV})$, [b] $E_{HOMO} = E_{LUMO} - E_{gap}^{optical}$, [c] optical HOMO-LUMO energy, [d] Theoretical calculation, [e] Peak potentials for **2**, **4**, **5**, **7** and **8** were not clearly resolved, [f] Theoretical treatments for **5**, **7** and **8** were not carried out, owing to limitations in suitably packaged basis sets for iodine.

It is important to note that the CV results illustrate the trend of lowering LUMO levels which is in the same order as energies predicted from theoretical calculations. The result of lowering energy gap obtained from UV-Vis experiments was also in the same order as the theoretically predicted values.

1.6. Conclusions

A straightforward synthetic route to asymmetrically substituted phenazine derivatives **1-8** was successfully established. ^{1}H and ^{13}C NMR and mass spectrometry analyses confirmed that the correct molecules were obtained. It was shown from UV-vis

spectroscopy that by changing the type (from H to F to Cl to Br to I) or position (from 2,3- to 1,4-) of halogen, the polarizability is increased and the absorption edge is pushed to longer wavelengths, which results in a decrease of the energy gap. This decrease of the energy gap is consistent with fluorescence spectra which also showed a red shift in the same order.

Cyclic voltammetry and theoretical calculations further corroborated that the electronic properties of the molecule, the electron affinity and HOMO-LUMO energy gap, can be modulated by changing different type or position of halogen substituents.

The length of alkyl group has no effect on the molecules' chromophores so that the electronic properties were almost the same among compounds **5**, **7** and **8**.

1.7. References

1. Hu, J.; Odom, T. W. and Lieber, C. M. "Chemistry and Physics in One Dimension: Synthesis and Properties of Nanowires and Nanotubes" *Acc. Chem. Res.* **1999**, *32*, 435-445.

2. Xia, Y.; Yang, P.; Sun, Y.; Wu, Y.; Mayers, B.; Gates, B.; Yin, Y.; Kim, F.; Yan, H. "One-dimensional nanostructures: Synthesis, characterization, and applications" *Adv. Mater.* **2003**, *15*, 353-389.

3. Wu, J.; Pisula, W.; Muellen, K. "Graphenes as potential material for electronics" *Chem. Rev.* **2007**, *107*, 718-747.

4. Schenning, A. P. H. J.; Meijer, E. W. "Supramolecular electronics; nanowires from self-assembled π-conjugated systems" *Chem. Commun.* **2005**, 3245-3258.

5. Nguyen, T. Q.; Martel, R.; Avouris, P.; Bushey, M. L.; Brus, L.; Nuckolls, C. "Molecular interactions in one-dimensional organic nanostructures" *J. Am. Chem. Soc.* **2004**, *126*, 5234-5242.

6. Wang, Z.; Medforth, C. J.; Shelnutt, J. A. "Porphyrin nanotubes by ionic selfassembly" *J. Am. Chem. Soc.* **2004**, *126*, 15954-15955.

7. Shirakawa, M.; Fujita, N.; Shinkai, S. "A stable single piece of unimolecularly π-stacked porphyrin aggregate in a thixotropic low molecular weight gel: A onedimensional molecular template for polydiacetylene wiring up to several tens of micrometers in length" *J. Am. Chem. Soc.* **2005**, *127*, 4164-4165.

8. Kulkarni, A. P.; Tonzola, C. J.; Babel, A.; Jenekhe, S. A. "Electron Transport Materials for Organic Light-Emitting Diodes" *Chem. Mater.* **2004**, *16*, 4556-4573.

9. Karastatiris, P.; Mikroyannidis, J. A.; Spiliopoulos, I. K.; Kulkarni, A. P.; Jenekhe, S. A. "Synthesis, Photophysics, and Electroluminescence of New Quinoxaline- Containing Poly(p-phenylenevinylene)s" *Macromolecules* **2004**, *37*, 7867-7878.

10. Kulkarni, A. P.; Zhu, Y.; Jenekhe, S. A. "Quinoxaline-Containing Polyfluorenes: Synthesis, Photophysics, and Stable Blue Electroluminescence" *Macromolecules* **2005**, *38*, 1553-1563.

11. Tonzola, C. J.; Alam, M. M.; Jenekhe, S. A. "A New Synthetic Route to Soluble Polyquinolines with Tunable Photophysical, Redox, and Electroluminescent Properties" *Macromolecules* **2005**, *38*, 9539-9547

12. Granstrom, M.; Petritsch, K.; Arias, A. C.; Lux, A.; Andersson, M. R.; Friend, R. H. "Laminated fabrication of polymeric photovoltaic diodes" *Nature* **1998**, *395*, 257-260.

13. Halls, J. J. M.; Walsh, C. A.; Greenham, N. C.; Marseglia, E. A.; Friend, R. H.; Moratti, S. C.; Homes, A. B. "Efficient photodiodes from interpenetrating polymer networks" *Nature* **1995**, *376*, 498-500.

14. Peng, Z.; Galvin, M. E. "Polymers with High Electron Affinities for Light-Emitting Diodes" *Chem. Mater.* **1998**, *10*, 1785-1788.

15. Bao, Z.; Lovinger, A. J.; Brown, J. "New Air-Stable n-Channel Organic Thin Film Transistors" *J. Am. Chem. Soc.* **1998**, *120*, 207-208.

16. Heidenhain, S. B.; Sakamoto, Y.; Suzuki, T.; Miura, A.; Fujikawa, H.; Mori, T.; Tokito, S.; Taga, Y. "Perfluorinated Oligo(p-Phenylene)s: Efficient n-Type Semiconductors for Organic Light-Emitting Diodes" *J. Am. Chem. Soc.* **2000**, *122*, 10240-10241.

17. Sakamoto, Y.; Komatsu, S.; Suzuki, T. "Tetradecafluorosexithiophene: The First Perfluorinated Oligothiophene" *J. Am. Chem. Soc.* **2001**, *123*, 4643-4644.

18. Pisula, W.; Tomovic, Z.; Simpson, C.; Kastler, M.; Pakula, T.; Mullen, K. "Relationship between Core Size, Side Chain Length, and the Supramolecular Organization of Polycyclic Aromatic Hydrocarbons" *Chem. Mater.* **2005**, *17*, 4296-4303

19. Yagai, S.; Kinoshita, T.; Higashi, M.; Kishikawa, K.; Nakanishi, T.; Karatsu, T.; Kitamura, A. "Diversification of Self-Organized Architectures in Supramolecular Dye Assemblies" *J. Am. Chem. Soc.* **2007**, *129*, 13277-13287.

20. Kastler, M.; Pisula, W.; Wasserfallen, D.; Pakula, T.; Müllen, K. "Influence of Alkyl Substituents on the Solution- and Surface-Organization of Hexa-peri-hexabenzocoronenes" *J. Am. Chem. Soc.* **2005**, *127*, 4286-4296.

21. Balakrishnan, K.; Datar, A.; Naddo, T.; Huang, J.; Oitker, R.; Yen, M.; Zhao, J.; Zang, L. "Effect of Side-Chain Substituents on Self-Assembly of Perylene Diimide Molecules: Morphology Control" *J. Am. Chem. Soc.* **2006**, *128*, 7390-7398.

22. Jancy, B.; Asha, S. K. "Hydrogen-Bonding-Induced Conformational Change from J to H Aggregate in Novel Highly Fluorescent Liquid-Crystalline Perylenebisimides" *Chem. Mater.* **2008**, *20*, 169-181.

23. van Gorp, J. J.; Vekemans, J. A. J. M.; Meijer, E. W. "C3-Symmetrical Supramolecular Architectures: Fibers and Organic Gels from Discotic Trisamides and Trisureas" *J. Am. Chem. Soc.* **2002**, *124*, 14759-14769.

24. Lee, D. C.; Jang, K.; McGrath, K. K.; Uy, R.; Robins, K. A.; Hatchett , D. W. "Self-Assembling Asymmetric Bisphenazines with Tunable Electronic Properties" *Chem. Mater.* **2008**, *20*, 3688-3695.

25. Lee, D. C.; McGrath, K. K.; Jang, K. "Nanofibers of asymmetrically substituted bisphenazine through organogelation and their acid sensing properties" *Chem. Commun.*, **2008**, 3636-3638

26. McGrath, K. K.; Jang, K.; Robins, K. A.; Lee, D. C. "Substituent Effect on the Electronic Properties and Morphologies of Self-Assembling Bisphenazine Derivatives" *Chem. Eur. J.* **2009**, *15*, 4070-4077

27. Jang, K.; Kinyanjui, J. M.; Hatchett, D. W.; Lee, D. C. "Morphological Control of One-Dimensional Nanostructures of T-Shaped Asymmetric Bisphenazine" *Chem. Mater.*, **2009**, Article ASAP.

28. Pozzo, J. L.; Clavier, G. M. and Desvergne, J. P. "Rational design of new acid-sensitive organogelators" *J. Mater. Chem.* **1998**, *8*, 2575-2577.

29. Bartholomew, G. P.; Bazan, G. C.; Bu, X.; Lachicotte, R. J. "Packing Modes of Distyrylbenzene Derivatives " *Chem. Mater.*, **2000**, *12*, 1422-1430.

30. An, B. K.; Gihm, S. H.; Chung, J. W.; Park, C. R.; Kwon, S. K.; Park, S. Y. "Color-Tuned Highly Fluorescent Organic Nanowires/Nanofabrics: Easy Massive Fabrication and Molecular Structural Origin" *J. Am. Chem. Soc.* **2009**, *131*, 3950-3957.

31. Zhu, Y.; Gibbons, K. M.; Kulkarni, A. P.; Jenekhe, S. A. "Polyfluorenes Containing Dibenzo[a,c]phenazine Segments: Synthesis and Efficient Blue Electroluminescence from Intramolecular Charge Transfer States" *Macromolecules* **2007**, *40*, 804-813.

32. Bundgaard, E.; Krebs, F. C. "Low-Band-Gap Conjugated Polymers Based on Thiophene, Benzothiadiazole, and Benzobis(thiadiazole)" *Macromolecules* **2006**, *39*, 2823-2831.

CHAPTER 2

ASSEMBLY

2.1. Introduction

Due to the potential applications in nanoscaled optoelectronic devices,[1] the 1-D SA of

π-conjugated organic semiconductors into nanofibers,[2-4] nanobelts,[5-7] and nanotubes[8-10]

with high aspect ratios has been one of the most active fields of research.

The morphological control of self-assembled nanostructure is worthy of particular

interest because it will directly influence the devices' performance.[11-13] There are several

ways to control the morphology based on a rational molecular design strategy. First, we

can manipulate the side groups bonded to π-cores such as altering the length[14-15] and

branching.[16-17] Secondly, we can control the assembly condition,[18] such as the assembly

method, the concentration and polarities of the solvent, or we can control the secondary

interactions.[19-20]

Organic supramolecular self-assemblies are often based on a combination of

noncovalent interactions, including van der Waals forces and π-π stacking, as well as

hydrogen bonding (HB).[21-22] HB interactions have been used to control the growth and

microstructure of films used in a variety of applications including nonlinear optics,

sensors, and transistors.[23-24] Interestingly, halogen bonding (XB) exhibits characteristics

similar to HB in directionality and strength. XB is an intermolecular interaction involving

a halogen atom (frequently iodine and bromine, but also chlorine and even fluorine) and a

neutral or anionic Lewis base.[25-26] Most of the previous research shows that XB plays an important role in natural systems[27] and has been used for crystal engineering, liquid crystals, and template synthesis.[28-32] However, to the best of our knowledge, XB as one of driving forces to control the morphology in solution based 1D self-assembly has never been accomplished.

In the first chapter, it has been demonstrated that the peripheral halogen substituents were effective at modifying the electronic properties of the whole system. In addition, those substituents are expected to influence the morphology of the 1-D nanostructures even with their trivial size. This chapter will focus on the morphological control through halogen effect, position effect, and alkyl length effect.

2.2. Experiments

2.2.1. Drop casting film

2.2.1.1. Drop casting film on cover glass

Cast films of compounds **1**-**8** were made as follows. First, each compound was dissolved in CH_2Cl_2; the solution was transferred with a pipette and drop-cast onto a clean cover glass surface. Then it was left undisturbed for several minutes, until the solvents evaporated. A raw crystalline structure of each compound was finally formed on top of the cover glasses. The castfilm experiment was carried out twice and the data is reproducible.

2.2.1.2. UV-vis absorption spectroscopy

The intermolecular π-π interactions in solid state were investigated with UV-vis spectroscopy. The UV-vis absorption spectra of the solid state samples of compounds **1** –

8 (drop casted thin films on cover glasses) were collected on a Shimadzu UV-2450 UV-vis spectrophotometer and compared with those in the solution state.

2.2.2. Phase transfer (PT) self-assembly

2.2.2.1. Phase transfer (PT) self-assembly in bisolvent system

The solution based SA was performed using a phase transfer (PT) method[7] in a CH_2Cl_2/methanol binary solvent system. All solvents were filtered through a 0.2 μm PTFE filter before each PT experiment. A homogeneous solution of the compound was prepared in a "good" solvent (CH_2Cl_2) and was filtered through a 0.2 μm PTFE filter into a clean 20 mL screw-cap vial. The "poor" solvent (methanol) was slowly added to the CH_2Cl_2 solution so that two phases could be maintained. The binary solvent mixture was then left undisturbed overnight to induce 1-D assembly. The volume ratio of CH_2Cl_2/methanol was kept constant (1/5 v/v).

2.2.2.2. Scanning electron microscopy (SEM)

The assembled product by PT was drop casted onto gold mica and the solvent was evaporated under ambient conditions. SEM images of the 1-D assembled samples were obtained on a Jeol JSM-5600 scanning electron microscope. Before imaging, all samples were sputter-coated (50 mA, 60 sec.) with a thin layer of gold to prevent charging. Accelerating voltages and working distances are specified with each image.

2.2.2.3. Single crystal X-ray crystallography

Single crystal X-ray crystallography was carried out with compound **3.** Crystals were prepared in 5 mM CH_2Cl_2 (2 mL) and MeOH (10 mL) binary solvent system. Single crystal diffraction data were collected on a microcrystal diffraction beamline (11.3.1) at the Advanced Light Source (supported by the Director, Office of Science, Office of Basic

Energy Science, of the US Department of Energy under Contract No. DEAC02-05CH11231). Needles were examined in paratone in a polarizing microscope, and a flat needle was selected that appeared to be unbent. Attempts to collect data at 100 K produced poor peak profiles and low quality data, indicating stress or a phase transition accompanying cooling. As a result, higher quality data were collected at room temperature. A full sphere of data was collected, and the structure was solved using direct methods and refined within the SHELXTL routine.[33] Hydrogen atoms were generated using the riding model, but no other restraints/constraints were necessary to refine the structure to an R_1 value of 4.09%. Statistics from the refinement are presented in Table 2.1.

2.2.2.4. Transmission electron microscopy (TEM)

The assembled product by PT was drop casted onto a 3 mm diameter carbon-coated copper grid using a pipette. A TECNAI-G2-F30 transmission electron microscope with a 300 KeV Schottky field emission gun was used to characterize the morphology and atomic structure of the molecules under the conventional diffraction contrast (bright-field, BF) and Z-contrast (scanning transmission electron microscope, STEM) modes.

2.2.2.5. X-ray diffraction (XRD)

The assembled product by PT was drop casted onto a zero background plate and the solvent was evaporated under ambient conditions. X-ray diffraction analyses were carried out on an X'Pert PRO PANalytical diffractometer at 25 ˚C using Cu-Kα radiation (λ = 1.54 Å, 40 KV, 40 mA).

2.2.2.6. High-resolution transmission electron microscopy (HRTEM)

The assembled sample by PT was drop casted onto a 3 mm diameter carbon film. The samples were left undisturbed for half an hour and ready for TEM observation. The same instrument was used as described in section 2.2.2.3. Many-beam condition was used to characterize the atomic structure under the phase-contrast (HRTEM) mode.

2.3. Results and Discussion

2.3.1. Drop casting film

2.3.1.1. UV-vis absorption spectroscopy

Figure 2.1. Normalized UV-vis spectra comparison of cast films (dash-dot lines) and solutions (solid lines) of final compounds **1** (A), **2** (B), **3** (C), **4** (D) and **5** (E).

The UV-vis absorption spectra of cast films of compounds **1–5** were recorded and compared with those in the solution state as shown in Figure 2.1. In general, cast film

samples showed significantly red-shifted absorption maxima compared with the absorptions in the solution state. This result strongly supports intermolecular π-π interactions in the solid state.
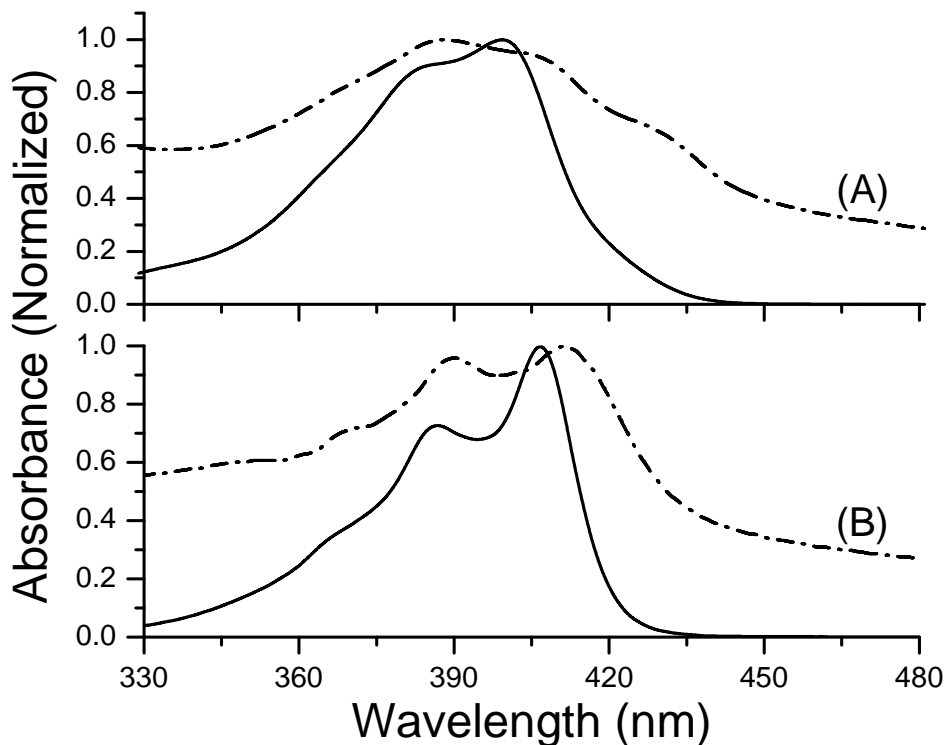
Figure 2.2. Normalized UV-vis spectra comparison of cast films (dash-dot lines) and solutions (solid lines) of final compounds **4** (B) and **6** (A).

While comparing the UV-vis spectra of cast films of **4** and **6**, the appearance of an additional shoulder around 435 nm in the case of **6** suggests more effective molecular π-aggregation in solid state. It is reasonable to assume that interactions between compound **6** through XB were geometrically more favored to induce a tight molecular packing due to 1,4-disubstitution, leading to more effective π orbital overlapping. Thus it has stronger π-π interactions between neighboring molecules than compound **4** and showed an additional shoulder at the higher wavelength.
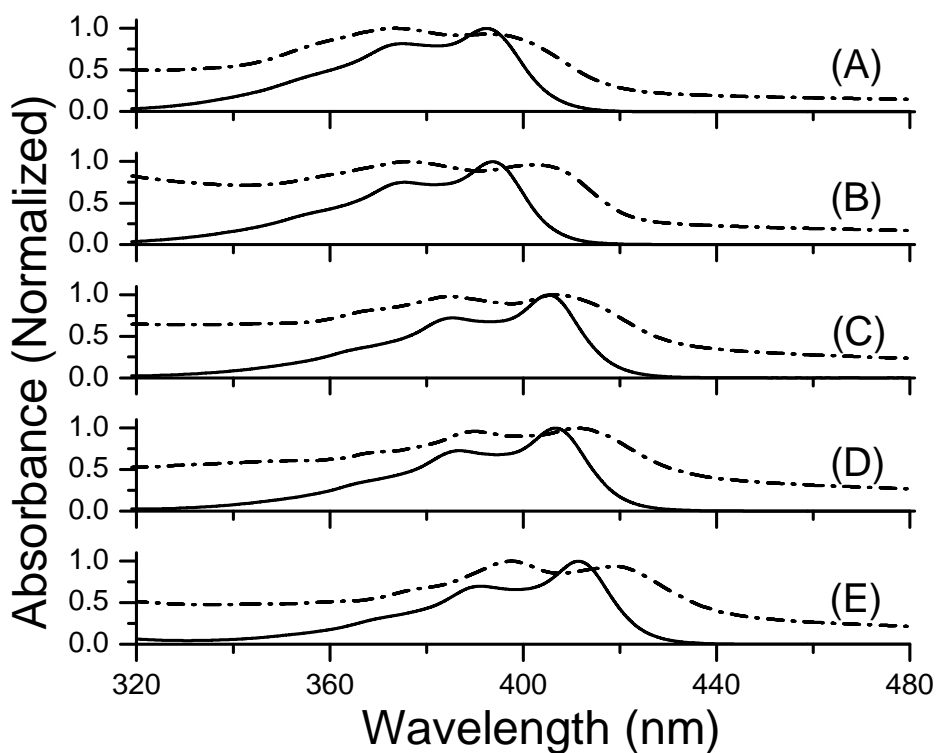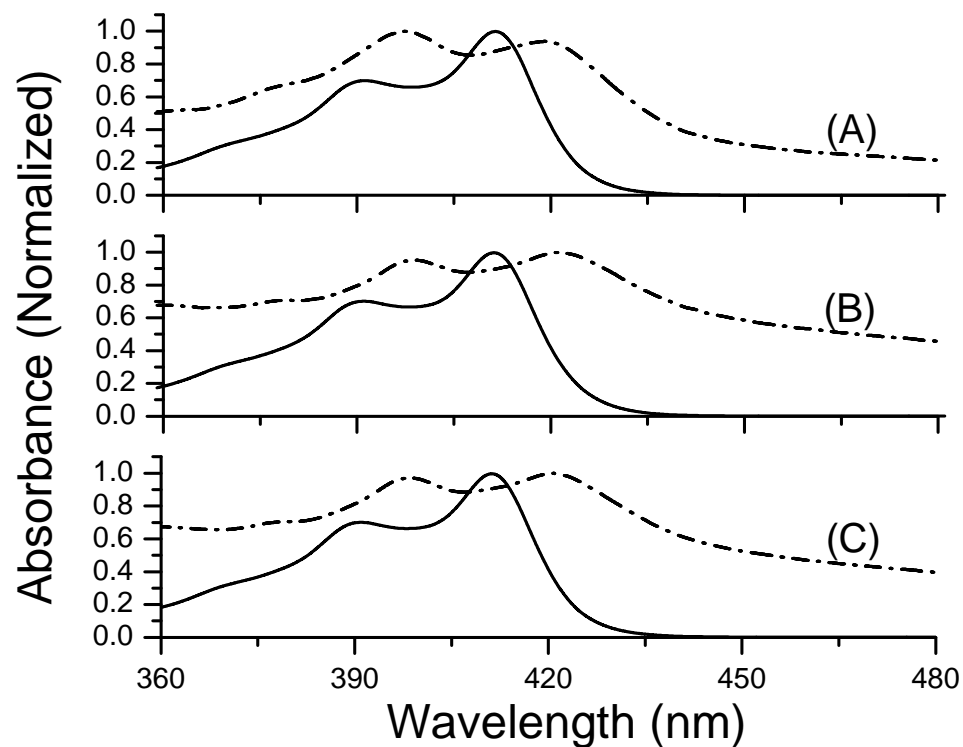
Figure 2.3. Normalized UV-vis spectra comparison of cast films (dash-dot lines) and solutions (solid lines) of final compounds **5** (A), **7** (B) and **8** (C).

All three iodine substituted compounds **5**, **7** and **8** showed similar behavior in both solution and solid state. The absorption maxima were significantly shifted to a longer wavelength from those of solution to cast films. All three spectra were nearly identical to each other. Therefore, the alkyl length has no influence to the optical properties of those compounds in both solution and solid state.

2.3.1.2. Polarized optical microscopy (POM)

The halogen effect on the morphology control of the

1-D nanoclusters formed on castfilms
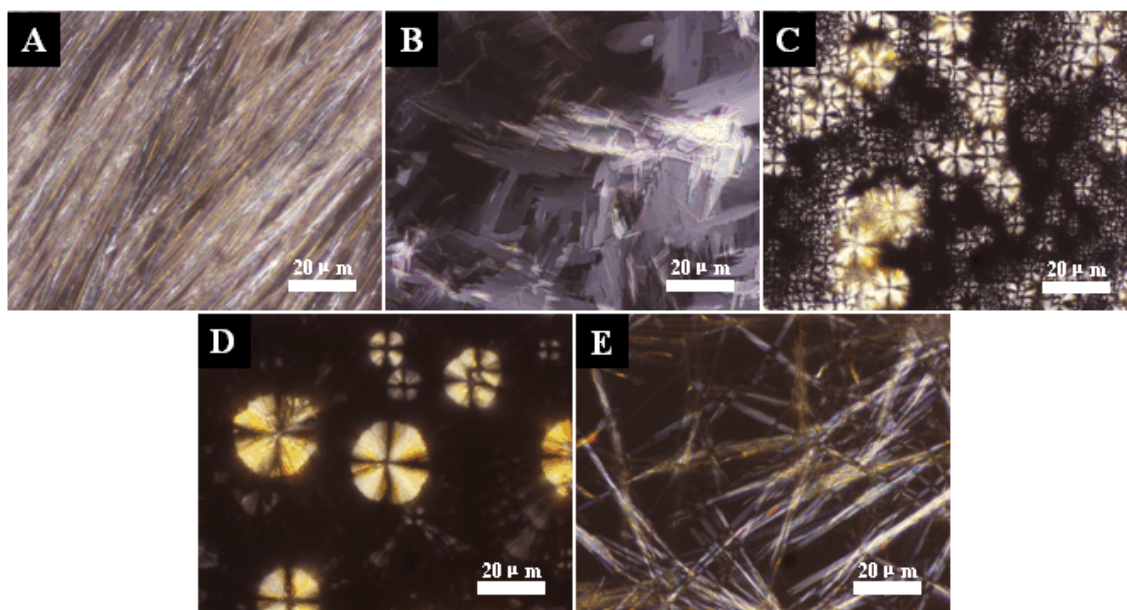
Figure 2.4. POM images of cast films of **1** (A), **2** (B), **3** (C), **4** (D) and **5** (E).
Scale bars: 20 μm.

Polarized optical microscopy (POM) was performed with these cast film samples **1-5** on cover glasses, as shown in Figure 2.4. Compounds **1** and **5** showed 1-D grown structures which means both of these two compounds have strong intermolecular interactions and produce a 1-D growth during the solvent evaporation process. In the case of compound **1**, the driving force could be HB while XB between iodine and the imine nitrogen might be the reason for compound **5**. Compound **2** showed random growth with a torn-paper like structure. Although fluorine has no XB, both HB and π-π interactions would be the major driving force and lead the molecules to grow in two directions. From images C and D, we can see the similar crystalline textures of compound **3** and **4**. In both

cases, the rate of nucleation could be much faster than that of 1-D fiber growth, both compound **3** and **4** showed spherulites structure.

<u>The position effect on the morphology control of the</u>

<u>1-D nanoclusters formed on castfilms</u>
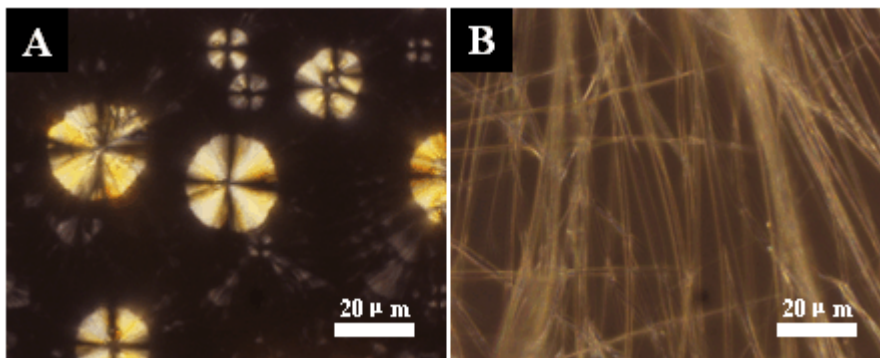
Figure 2.5. POM images of cast films of **4** (A) and **6** (B).
Scale bars: 20 μm.

POM comparison of cast films from compound **4** and **6** are shown in Figure 2.5. By changing the bromine group from the 2,3- (**4**) to 1,4-position (**6**), the cast film showed long 1-D grown microfibers instead of spherulites. This implies that for compound **6**, interactions between neighboring molecules is geometrically more favorable in one direction than compound **4**, resulting in the long fiber growth.
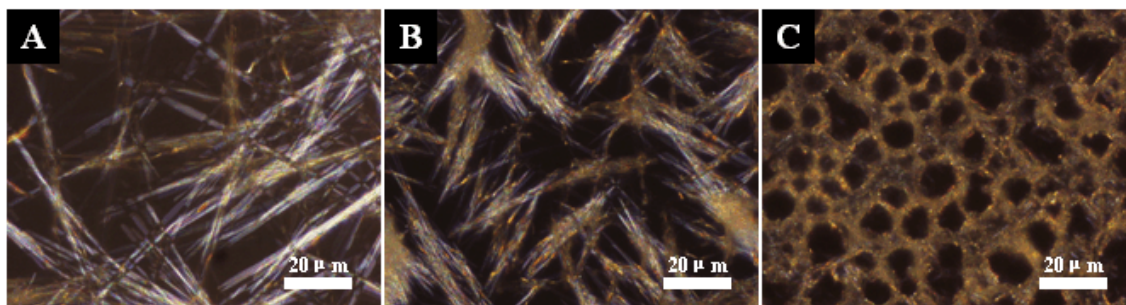
Figure 2.6. POM images of cast films of **5** (A), **7** (B) and **8** (C).
Scale bars: 20 μm.

POM comparisons of cast films from compounds **5, 7** and **8** are shown in Figure 2.6.

Both compounds **5** and **7** showed similar short needle-like structures, while compound **8**

with the longest alkoxyl chains (hexadecyloxy) in this series of molecules showed a cell-

like structure with numerous micro circles of various sizes all around the surface of the

cover glass. Although not clear, solvent trap followed by evaporation may be the reason

for the formation of the network structure.

2.3.2. Phase transfer (PT) self-assembly

2.3.2.1. Phase transfer (PT) self-assembly

The 1-D SA of compounds **1**–**8** were studied using both recrystallization from CH_2Cl_2 and a phase transfer (PT) method using two different binary solvent systems: CH_2Cl_2/methanol and CH_2Cl_2/hexane. The CH_2Cl_2/methanol binary solvent system was found to be more suitable for the assembly. Compound **1** showed no assembly due to its high solubility under the condition used. For the other compounds, a concentration study was carried out. To a homogeneous CH_2Cl_2 solution with a certain concentration (varying from 1 mM to 10 mM), methanol was added very slowly to maintain two phases. In all cases, the volume ratio between methylene chloride and methanol was kept constant (CH_2Cl_2/MeOH 1/5 v/v).

2.3.2.2. Scanning electron microscopy (SEM) Section I

<u>The halogen effect on the morphology control of the</u>

<u>1-D nanoclusters formed through PT</u>

The halogen substituent effect on the self-assembly properties of asymmetric phenazines **1**–**5** was examined by comparing the morphologies of the assembled structures obtained using SEM. Samples were prepared using PT method with all 5 mM concentration of CH_2Cl_2 solution.
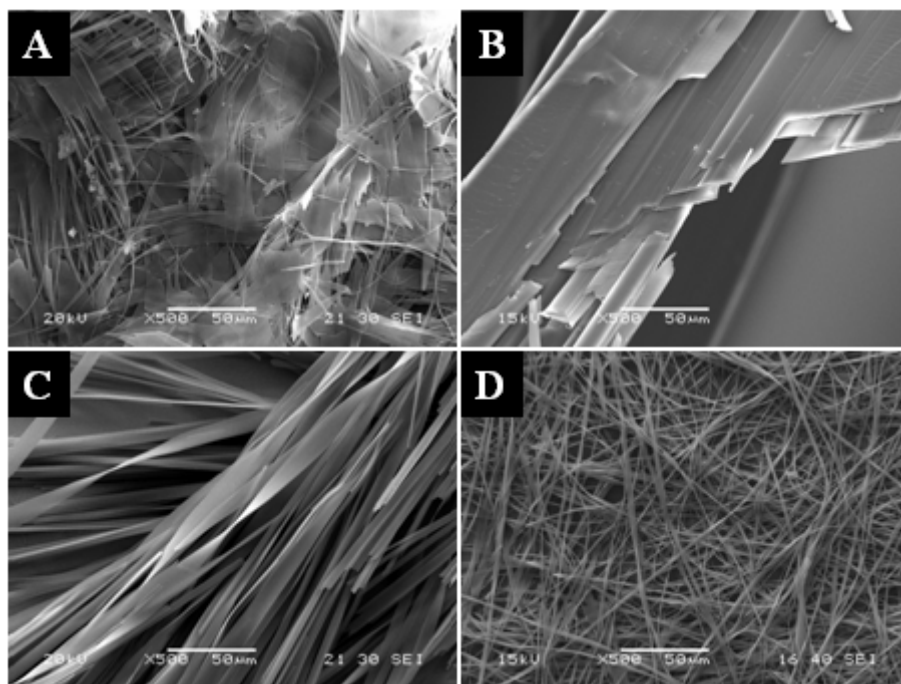
Figure 2.7. SEM images of PT assemblies of compounds **2** (A), **3** (B), **4** (C), and **5** (D). Scale bars: 50 μm.

Compound **1** did not form any assembled structure using the PT method due to its high solubility in the binary solvent system. As shown in the SEM images (Figure 2.7), fluorine containing phenazine (**2**) showed morphology similar to torn-paper. It was the most randomly assembled microstructures. Because of the small size of the fluorine atom, both π-π interactions and HB could be major driving forces, and their directions are perpendicular to each other. The fact that the structures can grow in two directions indicates the two interactions may have similar strength. For chlorine substituted phenazine (**3**), it formed large crystals, with the milimeters' length and width about 50 μm. From the single crystal X-ray crystallography (section 2.3.3.1), we confirmed that in the case of compound **3**, the major driving forces are HB, π-π interactions, and van der

Waals interactions. The detailed molecular packing will be discussed in the later section. Furthermore, both Br (**4**) and I (**5**) substituted phenazines showed a more 1-D character and the possible HB and the XB between halogens (typically Br or I) and imine nitrogens in **4** and **5** may exist simultaneously, serving together as the major driving force in these cases. The coexistence of HB and XB might be the reason that only compounds **4** and **5** formed twisted microbelts. Compared to the large crystal formed with compound **3**, the width of microbelts from both compounds **4** and **5** was much narrower, because the large size of bromine and iodine may hinder the lateral growth driven by π-π interactions.

2.3.2.3. Single crystal X-ray crystallography

Suitable crystals of compound **3** for single crystal X-ray crystallography measurements were obtained through the PT method at room temperature. Compound **3** forms in the Triclinic space group P-1 with the following unit cell dimensions: a = 5.421(2), b = 9.800(4), and c = 29.833(13) Å.
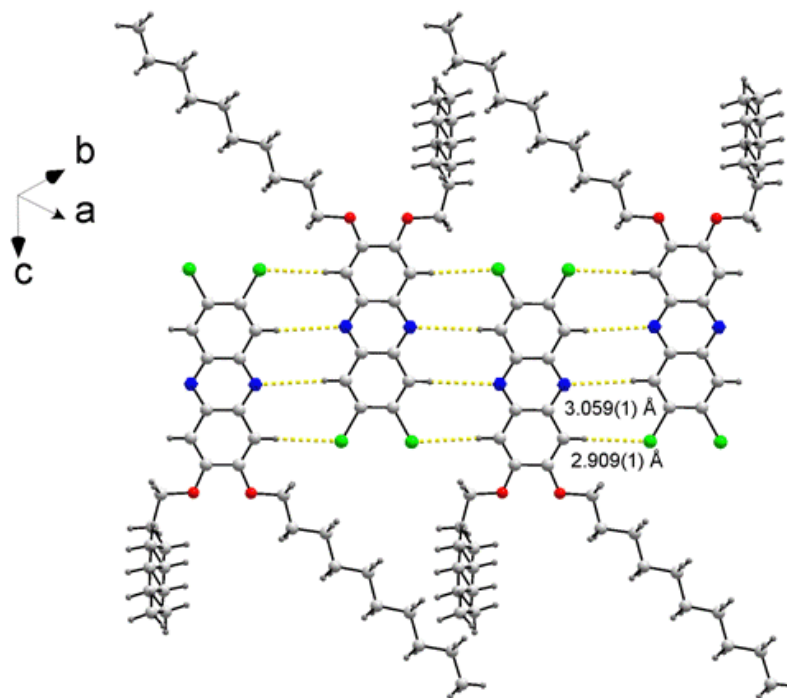
Figure 2.8. Crystal packing of compound **3**, shown as a ball and stick model, viewed along hydrogen bonding direction and showing short intermolecular contacts in dashed lines. Colors of atoms: carbon, grey; hydrogen, dark grey; nitrogen, blue; chlorine, green; oxygen, red.

The short intermolecular contacts are shown in Figure 2.8. In this crystal plane, both nitrogen and chlorine are involved in a HB interactions with hydrogen from the heteroaromatic ring of a phenazine moiety. Interestingly, the distance between iodine and a hydrogen from the alkoxy chain was only 2.92 Å, so there may be some weak interactions. Furthermore, in a single molecule, two alkyl chains are not in the same direction, one is mostly stretching in the same plane while another is pointing out of the plane.
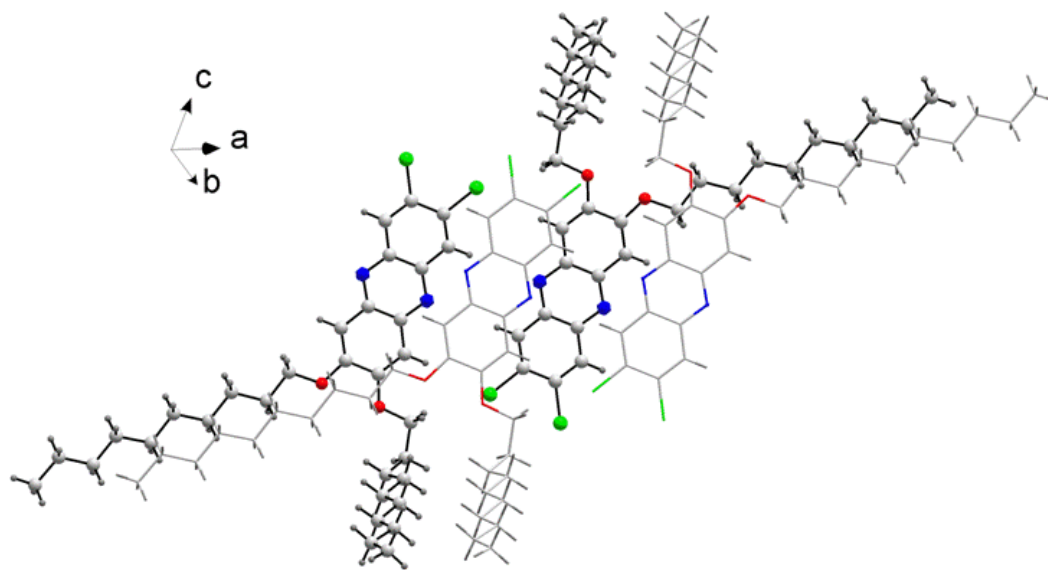
Figure 2.9. Crystal packing of compound **3**, viewed along hydrogen bonding direction and showing as two layered structure. Colors of atoms: carbon, grey; hydrogen, dark grey; nitrogen, blue; chlorine, green; oxygen, red.

As shown in Figure 2.9, it was confirmed that the molecule has an off-face stacking. Based on face indexing from single crystal X-ray crystallography, we conclude the *c* direction was mostly parallel to the long axis of the molecule. This direction is the less favored direction for self-assembly because van der Waals interactions between alkyl side groups are relatively weak. Strong HB interactions is closer to the *a* direction while π-π interactions would drive molecular growth in the direction closer to *b* which is clearly manifested in Figure 2.10.
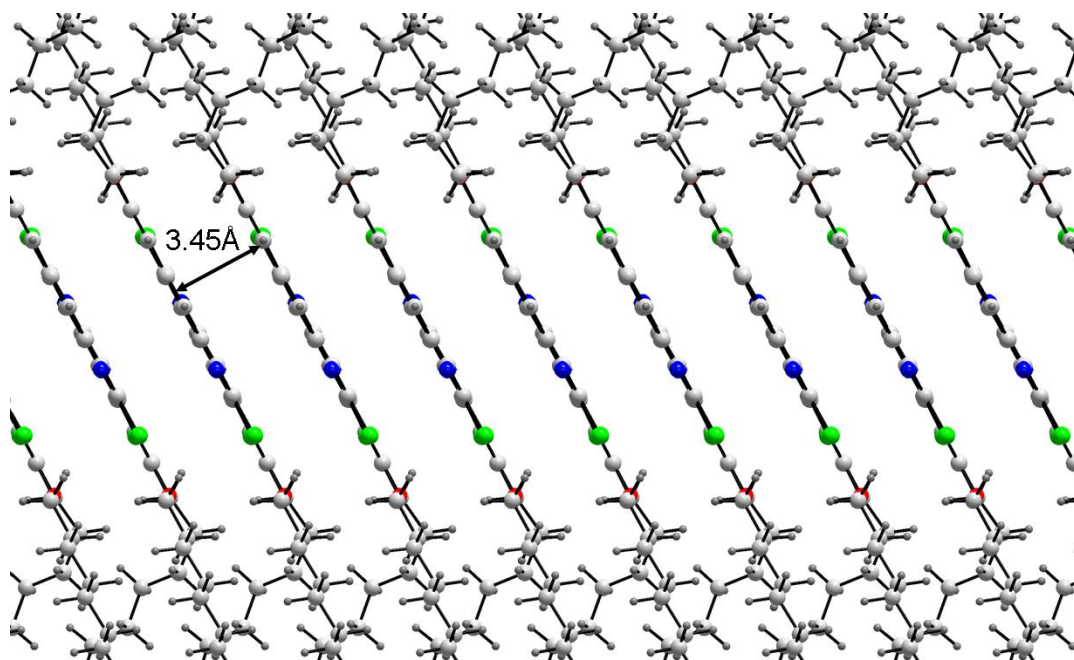
Figure 2.10. Crystal packing of compound **3** shown as a ball and stick model viewed along [210] direction. Colors of atoms: carbon, grey; hydrogen, dark grey; nitrogen, blue; chlorine, green; oxygen, red.

Parallel aligned molecular planes are illustrated from the [210] direction, as shown in Figure 2.10. The distance between the parallel planes is about 3.45 Å which is closer to typical π-π stacking distance.[34-35] Although the distance is short enough for π-π stacking, as mentioned earlier, off-face stacking may produce weak π-π interactions. As a result, the overall 3-D structure consists of continuous parallel molecular planes. HB, which is the strongest interaction in this case, drove the molecules to align side by side, growing in the major [210] direction and formed the long axis of the single crystal.

2.3.2.4. Scanning electron microscopy (SEM) Section II

The position effect on the morphology control of the

1-D nanoclusters formed through PT

Figure 2.11. SEM images of PT assemblies of compounds **4** (A, B) and **6** (C, D).
Scale bars: A, C are 500 μm. B, D are 50 μm.

To verify the existence of XB, SA structure of **4** and **6** were compared. Both compounds **4** and **6** produced assembled structures in the CH₂Cl₂/MeOH binary solvent system with a 3 mM CH₂Cl₂ solution. However, the morphologies were quite different from each other. In the case of compound **4,** thin and short microbelts were formed. Belt bundles varied in width from ≈2 μm to 10 μm. Compound **6** formed ultra long, straight microfibers rather than the short, twisted microbelts. Compared to compound **4**, compound **6** may have a more regular and stronger XB caused by a more favorable geometrical contact between bromine and imine nitrogen in neighboring molecules,

resulting in a better side by side molecular packing. In the case of compound **4**, halogen

bond angles make it difficult to generate long fibers.

<u>The alkyl length effect on the morphology control of the</u>

<u>1-D nanoclusters formed through PT</u>
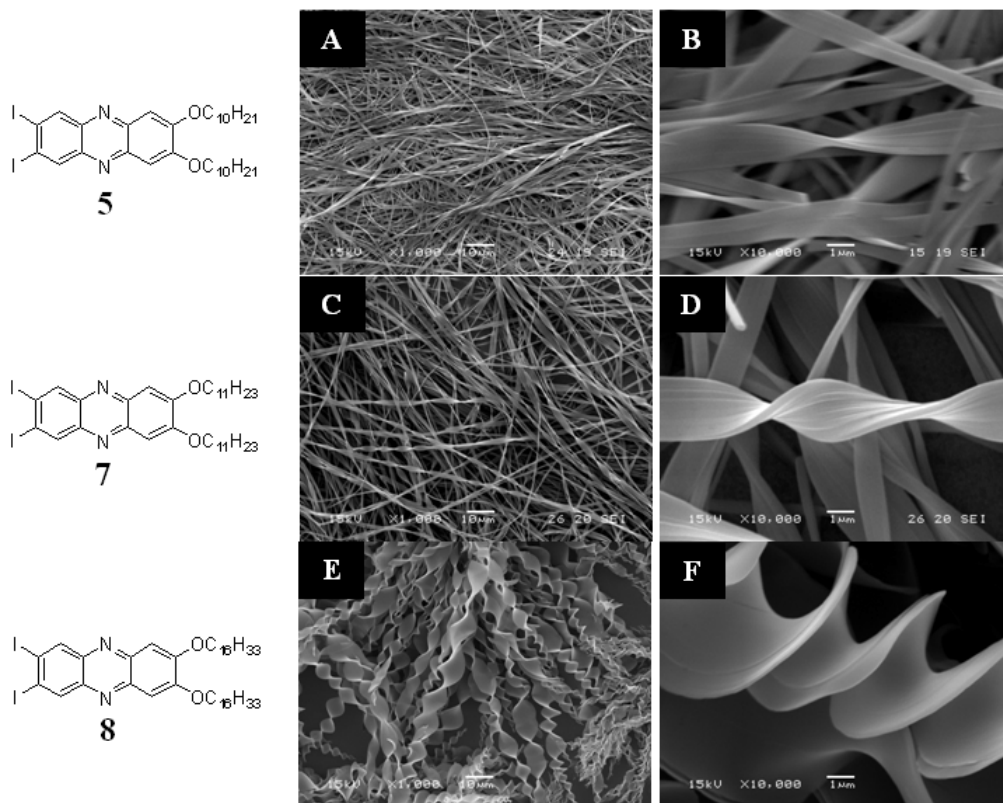
Figure 2.12. SEM images of PT assemblies of compounds **5** (A, B), **7** (C, D), and **8** (E, F). Scale bars: A, C, E are 10 μm. B, D, F are 1 μm.

Compounds **5** and **7** produced fairly homogeneous microbelts by PT method from

CH_2Cl_2/MeOH system. Due to the poor solubility of compound **8**, a nice whole twisted

structure was only found in a very low concentration (0.1mM of CH_2Cl_2 solution) while

in higher concentrations it showed a partially twisted structure. As shown in Figure 2.9,

both compounds **5** and **7** formed 1-D structures by PT with a 1 mM CH_2Cl_2 solution. The

width of the microbelts and the proportion of twisting obtained from compound **8** were much bigger and more numerous than those from compounds **5** and **7**. The widths of the microbelts obtained from compound **5** varied from ≈800 nm to 2 μm while those of **8** varied from 3 μm to 10 μm. It is important to notice that the pitch of twisted structure is smaller going from **5** to **7** to **8**. It has been reported that slower precipitation processes may result in larger pitch distance, and the driving force for twisting may derive from the imbalance of the growth rate between the edge and center.[36] The fact that compound **8** produced the most twisted microbelts with smallest pitch distance may be attributed to its longest alkyl side groups,[36] and they may cause less favored longitude fiber growth. Further investigation of this alkyl chain length effect is in progress.

2.3.2.5. Transmission electron microscopy (TEM)
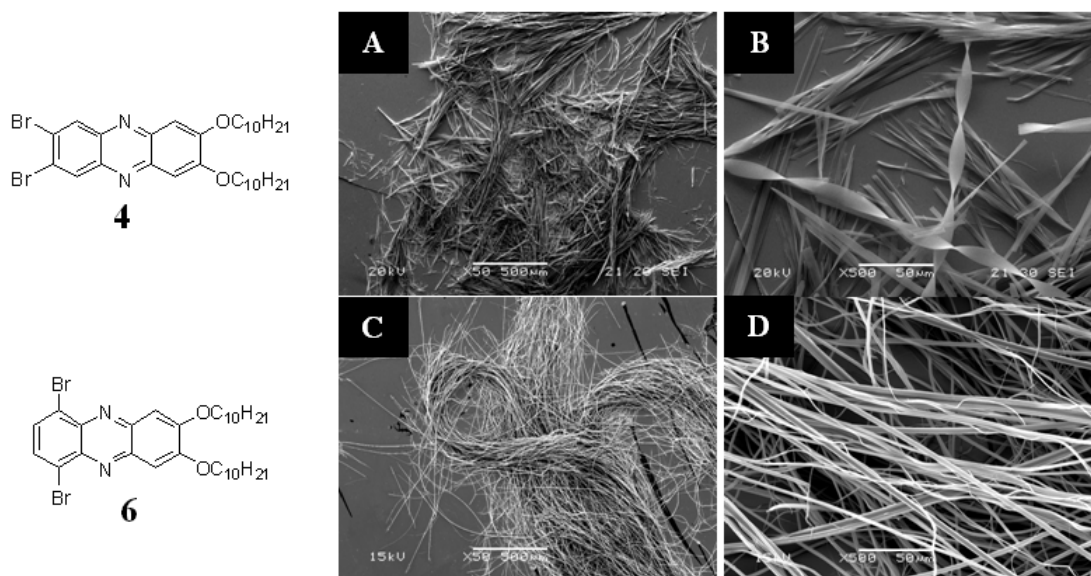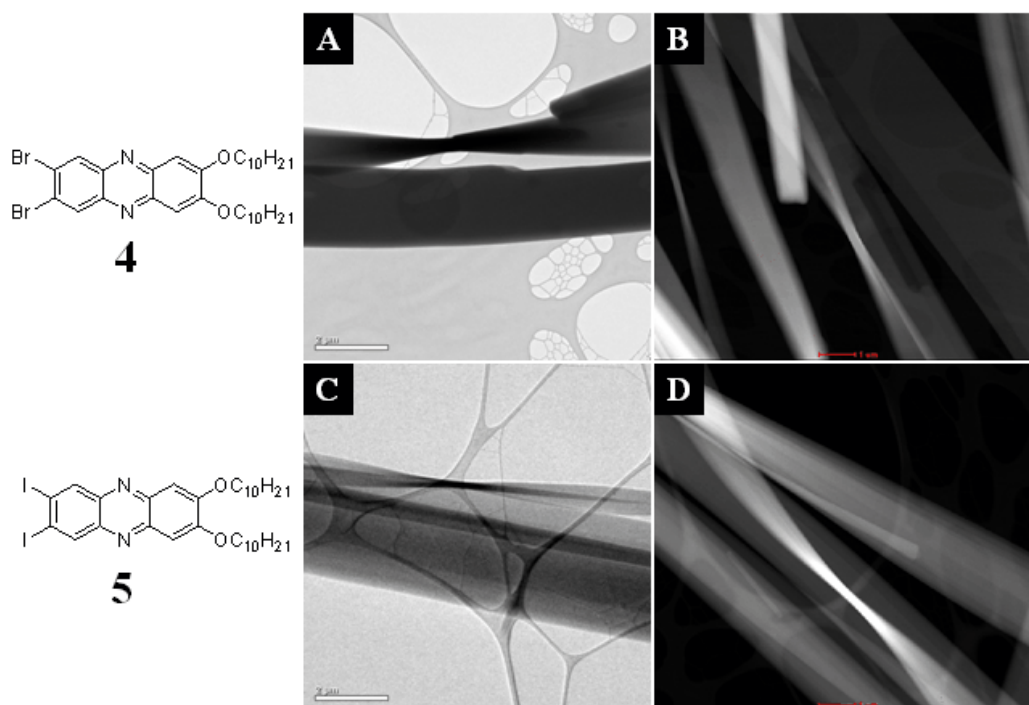

Figure 2.13. TEM images of PT assemblies of compounds **4** (A, B), and **5** (C, D). Scale bars: A, C are 2 μm. B, D are 1 μm.

Samples were prepared using PT with a 3 mM CH_2Cl_2 solution. From the BF and STEM mode images, we can see **4** and **5** have similar 1-D microstructure, in terms of width and length. The properties of bromine and iodine are similar to each other and there is some structural equivalence of halogen-bonded iodine and bromine,[37] so we expect that the molecular packing mode might be same. However, the microbelts of iodine substituted phenazine **5** looks thinner than the bromine substituted compound **4**, it may because the size of iodine is bigger than bromine, and XB between **5** is much stronger and the growth in the thickness direction is less favored compared with compound **4**.
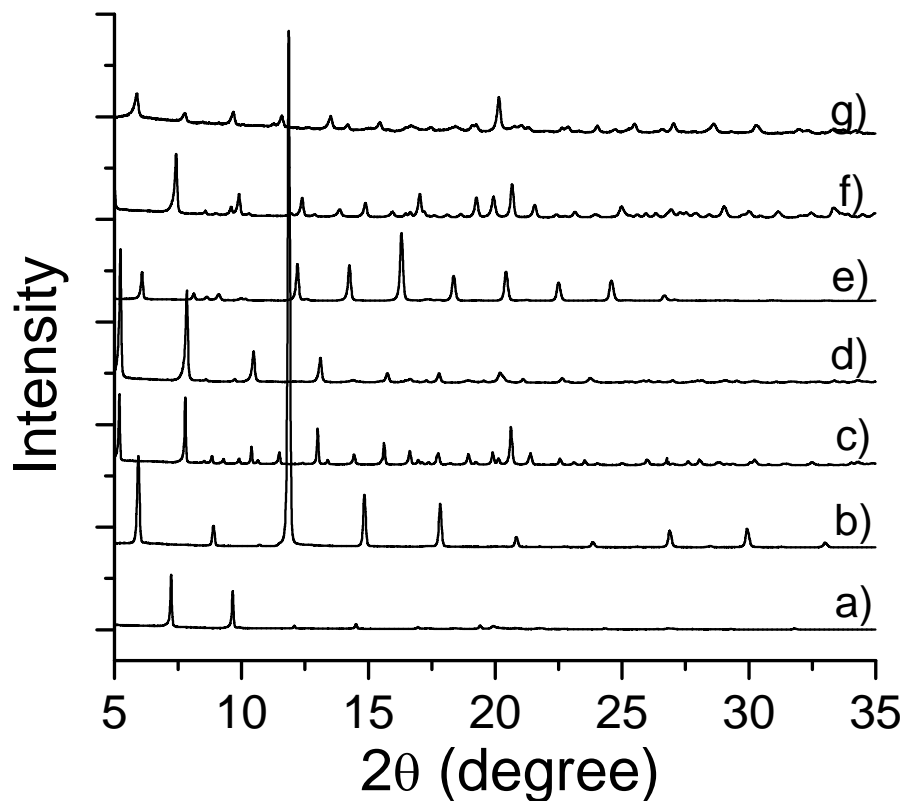
Figure 2.14. XRD patterns of PT assemblies of compounds **2** – **8** from CH_2Cl_2/MeOH. **2** (a), **3** (b), **4** (c), **5** (d), **6** (e), **7** (f), and **8** (g).

The XRD study was conducted on the self-assembled cluster of compounds **2**–**8**. Although XRD alone is not sufficient to deduce the molecular packing in the microclusters, the major purpose of this study was to determine the different crystallinity in these assembled samples.

The XRD patterns of the microstructures **2**-**6** obtained from the PT method from CH_2Cl_2/MeOH were compared to determine the effect of the peripheral halogen substituent on the 1-D self-assembly. All these five diffraction patterns show sharp, intense peaks, indicating that good crystallinity was found in these assembled samples.

Compounds **3** and **6**, which exhibit the highly ordered 1-D growing structure from SEM, showed the most well-defined diffraction pattern among the compounds, indicative of high crystallinity. Bromine substituted phenazine **4** showed a similar diffraction pattern as iodine substituted compound **5**, indicating similar molecular packing model which is consistent with the result observed in SEM images. In compound **2**, the XRD pattern was less defined and was not similar to other compounds. This may result from the random grown torn-paper like structure with a less order packing model.

In the case of compounds **7** and **8**, they show similar patterns to compound **5.** However, compound **8** shows lower intensity because a lower sample amount was used for XRD characterization.

2.3.3.7. High-resolution transmission electron microscopy (HRTEM)
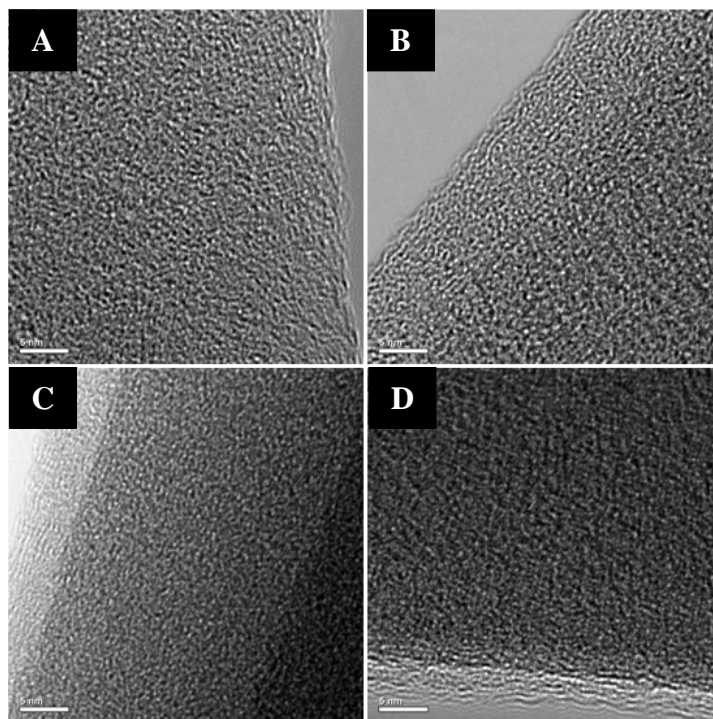
Figure 2.15. HRTEM images of compounds **2** (A), **4** (B), **5** (C), and **6** (D). Scale bars: 5 nm.

To further study the molecular packing model, HRTEM was carried out to investigate the molecular alignment. An electron diffraction pattern was not obtained because of irreproducibility of the data.

In general, similar alignments were observed in the edge area of compounds **4** and **6**, meanwhile compound **2** showed a less defined structure which is consistent with the XRD result. Only compound **5** showed a clear layered structure. At the edge area, it showed better longitude alignment while in the center it was less ordered because of the increasing thickness. Since the information from the HRTEM image is the accumulation of information from all different layers, the molecules may have better order in a single layer and show good crystallinity. However, they may align in different directions within different layers, resulting in a less ordered or even an amorphous texture on a larger scale.

2.4. Conclusion

We have demonstrated the utility of the halogen substituents in this series of asymmetric phenazine derivatives to induce 1-D assembly and manipulate the morphology of the self-assembled structures in terms of shape and size. SA using a phase transfer method with a methylene chloride/methanol binary solvent system showed that assembled morphologies are easily modified from 2-D torn-paper like structure to microbelts by changing different halogen peripheral substituents. Chlorine substituted phenazine **3**, which has HB interactions as the major driving force, resulted in the longest crystal structure among those five molecules (**1**-**5**). By changing the bromine substituents from 2,3- to 1,4-position, the ability to produce 1-D microfibers was enhanced. In addition, the length of alkyl group also influenced the morphology significantly. As the

alkyl length increased, the solubility was decreased, resulting in a whole twisted, short microbelt structure.

Combined analyses of SEM, TEM and XRD study identified the driving forces for the morphological transformation. The XRD patterns of all these compounds showed good crystallinity. In addition, the HRTEM result combined with the single crystal X-ray crystallography helped us to speculate the molecular packing models. As a result, collaboration of those different HB and XB interactions could be predominant and promote the molecules growing in a major direction. The results of this research illustrate a rational way for manipulating the electronic properties and assembly morphology of asymmetric phenazine, which has potential to be used in optoelectronic devices.

2.5. References

1. Briseno, A. L.; Mannsfeld, S. C. B.; Lu, X.; Xiong, Y.; Jenekhe, S. A.; Bao, Z.; Xia, Y. "Fabrication of Field-Effect Transistors from Hexathiapentacene Single-Crystal Nanowires" *Nano Lett.* **2007**, *7*, 668-675.

2. Hong, D. J.; Lee, E.; Lee, M. "Nanofibers from self-assembly of an aromatic facial amphiphile with oligo(ethylene oxide) dendrons" *Chem. Commun.* **2007**, 1801-1803.

3. Hamaoui, B. E.; Zhi, L.; Pisula, W.; Kolb, U.; Wu, J.; Mullen, K. "Self-assembly of amphiphilic imidazolium-based hexa-peri-hexabenzocoronenes into fibreous aggregates" *Chem. Commun.* **2007**, 2384-2386.

4. Kastler, M.; Pisula, W.; Wasserfallen, D.; Pakula, T.; Mullen, K. "Influence of Alkyl Substituents on the Solution and Surface-Organization of Hexa-peri-hexabenzocoronenes" *J. Am. Chem. Soc.* **2005**, *127*, 4286-4296.

5. Balakrishnan, K.; Datar, A.; Naddo, T.; Huang, J.; Oitker, R.; Yen, M.; Zhao, J.; Zang, L. "Effect of Side-Chain Substituents on Self-Assembly of Perylene Diimide Molecules: Morphology Control" *J. Am. Chem. Soc.* **2006**, *128*, 7390-7398.

6. Che, Y.; Datar, A.; Yang, X.; Naddo, T.; Zhao, J.; Zang, L. "Enhancing One-Dimensional Charge Transport through Intermolecular π-Electron Delocalization:

Conductivity Improvement for Organic Nanobelts" *J. Am. Chem. Soc.* **2007**, *129*, 6354-6355.

7. Che, Y.; Datar, A.; Balakrishnan, K.; Zang, L. "Ultralong Nanobelts Self-Assembled from an Asymmetric Perylene Tetracarboxylic Diimide" *J. Am. Chem. Soc.* **2007**, *129*, 7234-7235.

8. Hill, J. P.; Jin, W.; Kosaka, A.; Fukushima, T.; Ichihara, H.; Shimomoura, T.; Ito, K.; Hashizume, T.; Ishii, N.; Aida, T. "Self-Assembled Hexa-peri-hexabenzocoronene Graphitic Nanotube" *Science* **2004**, *304*, 1481-1483.

9. Kim, J. K.; Lee, E.; Lee, M. "Nanofibers with Tunable Stiffness from Self-Assembly of an Amphiphilic Wedge–Coil Molecule" *Angew. Chem., Int. Ed.* **2006**, *45*, 7195-7198.

10. Yamamoto, T.; Fukushima, T.; Yamamoto, Y.; Kosaka, A.; Jin, W.; Ishii, N.; Aida, T. "Stabilization of a Kinetically Favored Nanostructure: Surface ROMP of Self-Assembled Conductive Nanocoils from a Norbornene-Appended Hexa-peri- hexabenzocoronene" *J. Am. Chem. Soc.* **2006**, *128*, 14337-14340.

11. Ling, M. M.; Bao, Z. "Thin Film Deposition, Patterning, and Printing in Organic Thin Film Transistors" *Chem. Mater.* **2004**, *16*, 4824-4840.

12. Lim, J. A.; Lee, H. S.; Lee, W. H.; Cho, K. "Control of the Morphology and Structural Development of Solution-Processed Functionalized Acenes for High-Performance Organic Transistors" *Adv. Funct. Mater.* **2008**, *18*, 1-11.

13. Tsao, H. N.; Cho, D.; Andreasen, J. W.; Rouhanipour, A.; Breiby, D. W.; Pisula, W.; Mullen, K. "The Influence of Morphology on High-Performance Polymer Field-Effect Transistors" *Adv. Mater.* **2009**, *21*, 209-212

14. Pisula, W.; Tomovic, Z.; Simpson, C.; Kastler, M.; Pakula, T.; Mullen, K. "Relationship between Core Size, Side Chain Length, and the Supramolecular Organization of Polycyclic Aromatic Hydrocarbons" *Chem. Mater.* **2005**, *17*, 4296-4303

15. Yagai, S.; Kinoshita, T.; Higashi, M.; Kishikawa, K.; Nakanishi, T.; Karatsu, T.; Kitamura, A. "Diversification of Self-Organized Architectures in Supramolecular Dye Assemblies" *J. Am. Chem. Soc.* **2007**, *129*, 13277-13287.

16. Kastler, M.; Pisula, W.; Wasserfallen, D.; Pakula, T.; Müllen, K. "Influence of Alkyl Substituents on the Solution- and Surface-Organization of Hexa-peri-hexabenzocoronenes" *J. Am. Chem. Soc.* **2005**, *127*, 4286-4296.

17. Balakrishnan, K.; Datar, A.; Naddo, T.; Huang, J.; Oitker, R.; Yen, M.; Zhao, J.; Zang, L. "Effect of Side-Chain Substituents on Self-Assembly of Perylene Diimide Molecules: Morphology Control" *J. Am. Chem. Soc.* **2006**, *128*, 7390-7398.

18. Jiang, L.; Fu, Y.; Li, H.; Hu, W. "Single-Crystalline, Size, and Orientation Controllable Nanowires and Ultralong Microwires of Organic Semiconductor with Strong Photoswitching Property" *J. Am. Chem. Soc.* **2008**, *130*, 3937-3941.

19. Jancy, B.; Asha, S. K. "Hydrogen-Bonding-Induced Conformational Change from J to H Aggregate in Novel Highly Fluorescent Liquid-Crystalline Perylenebisimides" *Chem. Mater.* **2008**, *20*, 169-181.

20. van Gorp, J. J.; Vekemans, J. A. J. M.; Meijer, E. W. "C3-Symmetrical Supramolecular Architectures: Fibers and Organic Gels from Discotic Trisamides and Trisureas" *J. Am. Chem. Soc.* **2002**, *124*, 14759-14769.

21. Desiraju, G. R. "Crystal Engineering: A Holistic View" *Angew. Chem., Int. Ed.* **2007**, *46*, 8342-8356.

22. Schneider, H. J. "Mechanisms of Molecular Recognition: Investigations of Organic Host-Guest Complexes" *Angew. Chem., Int. Ed.* **1991**, *30*, 1417-1436.

23. Kim, C.; Facchetti, A.; Marks, T. J. "Polymer Gate Dielectric Surface Viscoelasticity Modulates Pentacene Transistor Performance" *Science* **2007**, *318*, 76-80.

24. Yoon, M.-H.; Facchetti, A.; Marks, T. J. "σ-π molecular dielectric multilayers for low-voltage organic thin-film transistors" *Proc. Natl. Acad. Sci. U.S.A.* **2005**, *102*, 4678-4682.

25. Metrangolo, P.; Resnati, G. "Halogen Bonding Based Recognition Processes: A World Parallel to Hydrogen Bonding" *Acc. Chem. Res.* **2005**, *38*, 386-395.

26. Metrangolo, P.; Resnati, G. "Halogen Bonding: A Paradigm in Supramolecular Chemistry" *Chem. Eur. J.* **2001**, *7*, 2511-2519.

27. Auffinger, P.; Hays, F. A.; Westhof, E.; Ho, P. S. "Halogen bonds in biological molecules" *Proc. Natl. Acad. Sci. U.S.A.* **2004**, *101*, 16789-16794.

28. Vartanian, M.; Lucassen, A. C. B.; Shimon, L. J. W.; van der Boom, M. E. "Cocrystallization of a Tripyridyl Donor with Perfluorinated Iodobenzene Derivatives: Formation of Different N---I Halogen Bonds Determining Network vs Plain Packing Crystals" *Cryst. Growth Des.* **2008**, *8*, 786-790.

29. Metrangolo, P.; Meyer, F.; Pilati, T.; Proserpio, D. M.; Resnati, G. "Highly Interpenetrated Supramolecular Networks Supported by N---I Halogen Bonding" *Chem. Eur. J.* **2007**, *13*, 5765-5772.

30. Glaser, R.; Knotts, N.; Yu, P.; Li, L. H.; Chandrasekhar, M.; Martin, C.; Barnes, C. L. "Perfect polar stacking of parallel beloamphiphile layers. Synthesis, structure and solid-

state optical properties of the unsymmetrical acetophenone azine DCA" *Dalton Trans.* **2006**, 2891-2899.

31. Reddy, C. M.; Kirchner, M. T.; Gundakaram, R. C.; Padmanabhan, K. A.; Desiraju, G. R. "Isostructurality, Polymorphism and Mechanical Properties of Some Hexahalogenated Benzenes: The Nature of Halogen---Halogen Interactions" *Chem. Eur. J.* **2006**, *12*, 2222-2234.

32. Caronna, T.; Liantonio, R.; Logothetis, T. A.; Metrangolo, P.; Pilati, T.; Resnati, G. "Halogen Bonding and π-π Stacking Control Reactivity in the Solid State" *J. Am. Chem. Soc.* **2004**, *126*, 4500-4501.

33. Sheldrick, G. M. "A short history of SHELX" *Acta Crystallogr. , Sect. A: Found. Crystallogr.* **2008**, *A64*, 112-122.

34. Schmidt-Mende, L.; Fechtenkotter, A.; Mullen, K.; Moons, E.; Friend, R. H.; MacKenzie, J. D. "Self-Organized Discotic Liquid Crystals for High-Efficiency Organic Photovoltaics" *Science* **2001**, *293*, 1119-1122.

35. Xiao, S.; Tang, J.; Beetz, T.; Guo, X.; Tremblay, N.; Siegrist, T.; Zhu, Y.; Steigerwald, M.; Nuckolls, C. "Transferring Self-Assembled, Nanoscale Cables into Electrical Devices" *J. Am. Chem. Soc.* **2006**, *128*, 10700-10701.

36. Chen, H. B.; Zhou, Y.; Yin, J.; Yan, J.; Ma, Y.; Wang, L.; Cao, Y.; Wang, J.; Pei, J. "Single Organic Microtwist with Tunable Pitch" *Langmuir* **2009**, *25*, 5459-5462.

37. Cincic, D.; Friscic, T.; Jones, W. "Structural Equivalence of Br and I Halogen Bonds: A Route to Isostructural Materials with Controllable Properties" *Chem. Mater.*, **2008**, *20*, 6623-6626.

APPENDIX CRYSTALLOGRAPHY DATA

Section 1. Crystal data and structure refinement for compound 3.

Empirical formula	$C_{32}H_{46}Cl_2N_2O_2$
Formula weight	561.61
Temperature	293(2) K
Wavelength	0.77490 Å
Crystal system	Triclinic
Space group	P-1
Unit cell dimensions	$a = 5.421(2)$ Å $\quad$ α= 90.125(6)
	$b = 9.800(4)$ Å $\quad$ β= 91.359(6)
	$c = 29.833(13)$ Å $\quad$ γ= 97.340(6)
Volume	1571.6(12) Å^3
Z	2
Density (calculated)	1.187 Mg/m^3
Absorption coefficient	0.294 mm^{-1}
F(000)	604
Crystal size	1.50 x 0.09 x 0.01 mm
Theta range for data collection	3.19 to 26.77°.
Index ranges	-6<=h<=6, -11<=k<=11, -34<=l<=34
Reflections collected	14611
Independent reflections	5164 [R(int) = 0.0393]
Completeness to theta = 26.77	99.5 %
Refinement method	Full-matrix least-squares on F^2
Data / restraints / parameters	5164 / 0 / 343
Goodness-of-fit on F^2	1.020
Final R indices [I>2sigma(I)]	$R_1 = 0.0409$, $wR_2 = 0.1089$
R indices (all data)	$R_1 = 0.0592$, $wR_2 = 0.1200$
Largest diff. peak and hole	0.187 and -0.252 e.Å^{-3}

Section 2. Atomic coordinates (x 10^4) and equivalent isotropic displacement parameters (Å^2 x 10^3) for compound 3. U(eq) is defined as one third of the trace of the orthogonalized U^{ij} tensor.

	x	y	z	U(eq)
Cl(1)	9484(1)	2290(1)	1116(1)	68(1)
O(2)	-295(2)	3614(1)	-1799(1)	55(1)
Cl(2)	4806(1)	76(1)	1122(1)	65(1)
O(1)	3406(2)	5496(1)	-1787(1)	54(1)
N(2)	6390(3)	3954(2)	-376(1)	51(1)
N(1)	2154(3)	1901(2)	-375(1)	52(1)
C(5)	3309(3)	4674(2)	-1422(1)	47(1)
C(6)	-3719(3)	2730(2)	-2275(1)	53(1)
C(7)	5241(3)	1180(2)	670(1)	49(1)
C(8)	1193(3)	3610(2)	-1427(1)	48(1)
C(9)	3546(4)	1095(2)	329(1)	52(1)
C(10)	7741(3)	3094(2)	325(1)	53(1)
C(11)	-2299(3)	2510(2)	-1846(1)	51(1)
C(12)	4685(3)	3841(2)	-708(1)	46(1)
C(13)	3870(3)	2016(2)	-36(1)	48(1)
C(14)	6002(3)	3039(2)	-37(1)	48(1)
C(15)	-9213(4)	606(2)	-2932(1)	63(1)
C(16)	-5760(4)	1556(2)	-2379(1)	57(1)
C(17)	-12616(4)	-326(2)	-3498(1)	69(1)
C(18)	-10716(4)	873(2)	-3353(1)	65(1)
C(19)	5484(4)	6567(2)	-1809(1)	54(1)
C(20)	2560(3)	2805(2)	-710(1)	47(1)
C(21)	5013(4)	7437(2)	-2210(1)	65(1)
C(22)	4988(3)	4769(2)	-1076(1)	50(1)
C(23)	851(3)	2713(2)	-1081(1)	51(1)
C(24)	7375(3)	2197(2)	669(1)	49(1)
C(25)	-7275(4)	1800(2)	-2799(1)	60(1)
C(26)	-14167(4)	-73(2)	-3911(1)	73(1)
C(27)	7308(4)	6310(2)	-2826(1)	65(1)

Section 2. (Continue)

C(28)	11338(5)	4191(3)	-4144(1)	86(1)
C(29)	6996(4)	5559(2)	-3274(1)	72(1)
C(30)	4854(4)	6677(2)	-2657(1)	66(1)
C(31)	8980(5)	4528(3)	-3934(1)	79(1)
C(32)	-15996(5)	-1299(3)	-4050(1)	93(1)
C(33)	-17617(6)	-1068(4)	-4455(1)	120(1)
C(34)	9376(4)	5247(3)	-3479(1)	77(1)
C(35)	10905(5)	3362(3)	-4574(1)	98(1)
C(36)	13233(6)	3041(4)	-4789(1)	122(1)

VITA

Graduate College
University of Nevada, Las Vegas

Bin Cao

Local address:
    1600 E University Ave, Apt 236.
    Las Vegas, Nevada 89119

Home Address:
    312 Hezuo Road,
    Shijiazhuang, Hebei, China 050051

Degrees:
    Bachelor of Engineering in Polymer Materials & Engineering,
    Zhengzhou University,
    Zhengzhou, China 450002

Thesis Title: Substituent Effect on the Electronic and Assembling Properties of
Asymmetric Phenazine Derivatives

Thesis Examination Committee:
    Chairperson, Dr. Dong-Chan Lee, Ph.D.
    Committee Member, Dr. Clemens Heske, Ph.D.
    Committee Member, Dr. Kathleen Robins, Ph.D.
    Graduate Faculty Representative, Dr. Michael Pravica, Ph.D.